arXiv:1607.04059v2 [hep-th] 1 Nov 2016

Monopole correlation functions and holographic phases of matter in 2+1 dimensions

T. Alho[a,1], V. Giangreco M. Puletti[a,2], R. Pourhasan[a,3], L. Thorlacius[a,b,4],

[a] *University of Iceland, Science Institute, Dunhaga 3, 107 Reykjavik, Iceland*

[b] *The Oskar Klein Centre for Cosmoparticle Physics, Department of Physics, Stockholm University, AlbaNova University Centre, 10691 Stockholm, Sweden*

Abstract

The strong coupling dynamics of a 2+1 dimensional U(1) gauge theory coupled to charged matter is holographically modeled via a top-down construction with intersecting D3- and D5-branes. We explore the resulting phase diagram at finite temperature and charge density using correlation functions of monopole operators, dual to magnetically charged particles in the higher-dimensional bulk theory, as a diagnostic.

[1] alho@hi.is
[2] vgmp@hi.is
[3] razieh@hi.is
[4] lth@hi.is

Contents

1 Introduction **3**

2 Monopole correlators at finite temperature **6**

2.1 Probe D5-brane in a black 3-brane background 6

2.2 Monopole two-point function 9

3 Finite charge density phase **16**

3.1 Thermodynamics of charged D5-branes 16

3.2 Monopole two-point function at finite charge density 20

4 Discussion **23**

A Action functionals for probe D-branes **25**

A.1 D5-brane 26

A.2 D3-brane 27

B Boundary counter-terms for D5-brane **29**

C On-shell D3-brane action **29**

D Asymptotic limits **32**

D.1 D5 limits 33

D.2 D3 limits 37

1 Introduction

Gauge/gravity duality provides an interesting setting for the study of compressible quantum phases, where strongly correlated quantum dynamics is encoded into space-time geometry in a gravitational dual description. The best understood cases all involve supersymmetric Yang-Mills theories in a large N limit, which are rather exotic from the point of view of many-body physics. Emergent gauge fields are known to arise in various quantum critical systems but these are almost exclusively U(1) fields and do not immediately lend themselves to a large N treatment. Gauge/gravity duality does, however, offer a rare glimpse into strongly coupled dynamics in a setting where explicit computations are relatively straightforward and some aspects of the dynamics, in particular at finite temperature and density, may be generic to more general strongly coupled field theories.

Motivated by recent work of N. Iqbal [1], we apply the formalism of gauge/gravity duality to map out the phase diagram of a 2+1-dimensional many body system with a conserved U(1) current at finite temperature and charge density. We use correlation functions of suitably defined magnetic monopole operators to probe the relevant physics [1, 2]. The fact that magnetic monopoles can strongly influence the infrared behavior of gauge theories is well known. For instance, the key role of monopoles in precipitating confinement in 2+1 dimensional gauge dynamics was emphasized in the pioneering work of Polyakov [3]. In a condensed matter context, monopoles provide an order parameter for the transition from anti-ferromagnetic order to valence bond solid in a gauge theory description of certain two-dimensional lattice anti-ferromagnets [4]. The phase transition is continuous and described by a $\mathbb{C}P^N$ model with monopoles condensing at the critical point, which has motivated the computation of monopole correlation functions in the $\mathbb{C}P^N$ model in a $1/N$ expansion [5].[1]

In a 2+1-dimensional gauge theory, a magnetic monopole operator, $\mathcal{M}(x_m)$, corresponds to a localized defect where a magnetic flux is inserted. Such operators belong to a more general class of topological disorder operators [7]. Their construction in terms of singular boundary conditions in a path integral formalism is outlined in [1]. Due to flux quantization, monopole operators are intrinsically non-perturbative and difficult to handle using conventional field theory techniques. In holography, on the other hand, correlation functions of monopole operators have a straightforward geometric representation and can be numerically evaluated using relatively simple methods.

The holographic description of magnetic monopole operators, in terms of intersecting D-branes, that we will be using was developed in [1, 8].[2] The starting point for the construction is a well-known top-down model for a 2+1-dimensional field theory living

[1] See [6] for a study of monopole operators by means of $4-\epsilon$ expansion.

[2] For other works related to holographic monopoles, see *e.g.* [9].

on the intersection of a single D5-brane and a large number N of coincident D3-branes [10]. In this model, the D5-brane is treated as a probe brane in the $AdS_5 \times S^5$ background geometry sourced by the D3-branes. The embedding of the D5-brane into the D3-brane geometry is obtained by minimizing the DBI action of the D5-brane in an $AdS_5 \times S^5$ background (we review the calculation in Section 2.1). There exists a solution where the D5-brane wraps an S_2 of fixed radius inside the S_5 and extends along an AdS_4 subspace of the AdS_5. This corresponds to a conformally invariant state in the dual 2+1-dimensional boundary theory. There are other solutions where the D5-brane embedding caps off at a finite radial coordinate, corresponding to a deformation away from criticality and a mass gap in the 2+1-dimensional theory.

Open strings stretching between the D3- and D5-branes give rise to matter fields in the fundamental representation of the SU(N) gauge group that are localised on the 2+1-dimensional intersection. The boundary theory also has a conserved global U(1) current, which corresponds under gauge/gravity duality to a bulk U(1) gauge field living in AdS_4. In general, a monopole operator inserted at the 2+1-dimensional boundary corresponds to a bulk field carrying magnetic charge under the bulk gauge field [11, 12]. In the top-down construction of [1] the monopoles are realized as a probe D3-brane, oriented in such a way as to appear as a one-dimensional curve in AdS_4, with the remaining world-volume coordinates filling (at most) half an S^3 in S^5 and ending on the S^2 wrapped by the D5-brane. A D($p-2$)-brane ending on a Dp-brane carries magnetic charge in the Dp world-volume [13] and thus the probe D3-brane represents a magnetically charged particle in AdS_4. If the D3 curve reaches the AdS_4 boundary at a point x_m, it corresponds to an insertion of a magnetic flux at that point, *i.e.* a boundary monopole operator. We review the construction in more detail in Section 2.2 and extend it to finite temperature backgrounds.

In the large N limit, the two-point function of boundary monopole operators is given by the on-shell D3 action,

$$\langle \mathcal{M}(\Delta x)\mathcal{M}^\dagger(0)\rangle \sim e^{-S_{D3}[\Delta x]}\,. \tag{1.1}$$

The D3-brane action consists of the usual DBI term and a magnetic coupling term. The DBI term is proportional to the length of the curve in AdS_4 traced out by the D3-brane, in a metric that depends on the D5-brane embedding, while the remaining term involves the integral of the magnetic dual of the world-volume gauge field along the same curve. The magnetic coupling will play a key role when we consider backgrounds at finite charge density.

In a charge gapped phase monopoles are expected to condense at large enough separation, that is their equal-time two-point function is expected to saturate with distance between the monopole insertion points [11]. In a Fermi-liquid phase (a compressible phase with non-zero charge density and no broken symmetries), field theory compu-

tations become rather involved due to the non-perturbative nature of the monopoles but [14] predicted a faster than power-law falloff for the monopole equal-time two-point function. This behaviour was indeed found in the holographic computation in [1], which gave a constant value for the monopole correlation as a function of distance in a charge gapped case, and a Gaussian falloff at large separation in a compressible phase.

Our goal is to understand how turning on a non-zero temperature affects monopole correlation functions. In particular, we wish to determine whether the spatial dependence of the monopole equal-time two-point function can still serve as an order parameter for phase transitions at finite T. Our starting point is the holographic model employed in [1], except now the D3-brane background is an AdS_5-Schwarzschild$\times S^5$ black brane, and we investigate the behavior of monopole correlation functions across the rather rich phase diagram spanned by temperature and charge density. Similar questions can in principle be addressed in other holographic models, including various phenomenologically motivated bottom-up models. It would be interesting to pursue this in future work but for now we will take advantage of the higher-dimensional geometric perspective provided by the specific top-down construction of [1].

The paper is organized as follows. In Section 2 we review the D3/D5-brane construction at finite temperature. We then introduce a monopole D3-brane and compute the D3-brane action that gives the monopole two-point function. In Section 3 we turn to the Fermi-liquid phase at finite charge density. After briefly introducing the relevant background D3/D5-brane solutions, we proceed to the D3-brane action, and map out the corresponding phase diagram. We conclude with a brief discussion in Section 4. Our conventions and definitions of the action functionals governing the probe D-brane dynamics studied in the paper are collected in Appendix A. This is followed in Appendix B by a short discussion of the boundary counter-terms that are required for the regularisation of the D5-brane free energy. A detailed examination of the on-shell D3-brane action at finite charge density and temperature is carried out in Appendix C and referred to in the main text. In Appendix D we consider asymptotic limits of model parameters, where analytic results can be obtained. This complements the numerical investigation in the rest of the paper and provides a useful check on the numerics.

2 Monopole correlators at finite temperature

2.1 Probe D5-brane in a black 3-brane background

Throughout the paper we consider probe D-branes in the finite temperature near-horizon geometry of N D3-branes,

$$ds^2 = \frac{u^2}{L^2}\Big[-h(u)\,dt^2+dx^2+dy^2+dx_\perp^2\Big]+\frac{L^2}{u^2}\Big[\frac{du^2}{h(u)}+u^2(d\psi^2+\sin^2\psi\,d\Omega_2^2+\cos^2\psi\,d\tilde{\Omega}_2^2)\Big], \tag{2.1}$$

where $h(u) = 1-(u_0/u)^4$, $d\Omega_2^2 = d\theta^2+\sin^2\theta d\phi^2$, $d\tilde{\Omega}_2^2 = d\tilde{\theta}^2+\sin^2\tilde{\theta}d\tilde{\phi}^2$, and L is a characteristic length scale. In these coordinates there is an event horizon at $u=u_0$ and the asymptotic AdS_5 boundary is at $u\to\infty$. The Hawking temperature is

$$T = \frac{u_0}{\pi L^2}\,, \tag{2.2}$$

and we note that a rescaling of T can be absorbed by a rescaling of the u coordinate. We work in the supergravity limit, so in particular at very large N, and insert a probe D5-brane with an AdS_4-Schwarzschild $\times$ S^2-embedding.[3] In the static gauge the D5-brane world-volume coordinates are $(t,x,y,u)\in$ AdS_4-Schwarzschild $\subset$ AdS_5-Schwarzschild and $(\theta\,,\phi)\in S^2\subset S^5$, as indicated in Table 1. The D5-brane profile is described by two functions, $x_\perp(u)$ and $\psi(u)$, that, due to translation and rotation symmetries in the world-volume directions, only depend on the radial coordinate u. We set $x_\perp=0$ throughout and focus on the angle $\psi(u)$, which controls the size of the 2-sphere wrapped by the probe D5-brane.[4] The D5-brane introduces matter fields in the fundamental representation of SU(N), charged under a global $U(1)_B$ (baryon number), and localized in (2+1)-dimensions. This is the field theory we have in mind throughout the paper.

Table 1: Background D-brane construction.

	t	x	y	$x_\perp$	u	ψ	θ	ϕ	$\tilde{\theta}$	$\tilde{\phi}$
N D3-branes (background)	×	×	×	×						
D5-brane (probe)	×	×	×		×		×	×		

For numerical computations, we find it convenient to introduce a dimensionless radial coordinate υ as follows [19]:

$$(u_0\upsilon)^2 = u^2+\sqrt{u^4-u_0^4}\,. \tag{2.3}$$

[3] D3/D5 systems at finite temperature and at finite chemical potential have been widely employed in applied holography [15, 16]. For reviews see [17].

[4] In Section 3 we consider a D5-brane carrying non-vanishing charge density. The ansatz $x_\perp=0$ remains consistent in this case as well, as long as the charge density is uniform. The stability of the configuration was studied in [18].

The horizon is at $\upsilon = 1$ and the background metric (2.1) becomes

$$ds^2 = \frac{1}{2}\left(\frac{u_0\upsilon}{L}\right)^2\left[-\frac{f^2}{\tilde{f}}\,dt^2 + \tilde{f}\,(dx^2{+}dy^2{+}dx_\perp^2)\right] + \frac{L^2}{\upsilon^2}\left(d\upsilon^2 + \upsilon^2\,d\Omega_5^2\right)\,, \tag{2.4}$$

where $f(\upsilon) = 1 - 1/\upsilon^4$ and $\tilde{f}(\upsilon) = 1 + 1/\upsilon^4$. The AdS boundary is at $\upsilon \to \infty$.

Writing $\chi(\upsilon) \equiv \cos\psi(\upsilon)$, the induced metric on the D5-brane is given by

$$ds^2 = \frac{1}{2}\Big(\frac{u_0\upsilon}{L}\Big)^2\Big[-\frac{f^2}{\tilde{f}}\,dt^2{+}\tilde{f}\,(dx^2+dy^2)\Big] + \frac{L^2}{\upsilon^2}\left(\frac{1-\chi^2+\upsilon^2\dot{\chi}^2}{1-\chi^2}\right)d\upsilon^2 + L^2\Big(1-\chi^2\Big)d\Omega_2^2\,, \tag{2.5}$$

where the dot denotes a derivative with respect to υ. The Euclidean DBI action for the probe D5-brane (see Appendix A) reduces to

$$I_{D5} = \mathcal{K}\,T^2\int \mathrm{d}\upsilon\,\upsilon^2 f\sqrt{\tilde{f}\,(1-\chi^2)\,(1-\chi^2+\upsilon^2\dot{\chi}^2)}\,, \tag{2.6}$$

with the constant $\mathcal{K}$ given in (A.10).

The field equation for χ,

$$\ddot{\chi} + \frac{\upsilon(3\upsilon^8+2\upsilon^4+3)\dot{\chi}^3}{(\upsilon^8-1)(1-\chi^2)} + \frac{3\chi\dot{\chi}^2}{1-\chi^2} + \frac{2(2\upsilon^8+\upsilon^4+1)\dot{\chi}}{\upsilon(\upsilon^8-1)} + \frac{2\chi}{\upsilon^2} = 0\,, \tag{2.7}$$

can be solved numerically using standard methods. There are two classes of solutions with a non-trivial $\chi(\upsilon)$ profile depending on whether the probe D5-brane extends all the way to the horizon at $\upsilon = 1$ or caps off outside the horizon. The former are referred to as "Black Hole Embedding" (BHE) solutions and the latter are so-called "Minkowski Embedding" (ME) solutions [20, 21]. A one-parameter family of black hole embedding solutions, with $0 \le \chi_0 \le 1$, is obtained by numerically integrating the field equation (2.7) from $\upsilon = 1$ outwards using the initial values $\chi(1) = \chi_0$, $\dot{\chi}(1) = 0$. The condition on $\dot{\chi}(1)$ comes from requiring the field equation to be non-singular at the horizon.

For the Minkowski embedding solutions, the numerical evaluation is streamlined by a further change of variables. By viewing υ and ψ as polar coordinates, the metric on S^5 may be rewritten as follows,

$$\begin{aligned} d\upsilon^2 + \upsilon^2\,d\Omega_5^2 &= d\upsilon^2 + \upsilon^2(d\psi^2 + \sin^2\psi\,d\Omega_2^2 + \cos^2\psi\,d\tilde{\Omega}_2^2) \\ &= dr^2 + r^2\,d\Omega_2^2 + dR^2 + R^2\,d\tilde{\Omega}_2^2\,, \end{aligned} \tag{2.8}$$

with

$$\upsilon^2 = r^2 + R^2, \qquad r = \upsilon\sin\psi, \qquad R = \upsilon\cos\psi\,. \tag{2.9}$$

In the new coordinates the D5-brane profile is described by a function $R(r)$ and a Minkowski embedding solution caps off at $r = 0$. The field equation (2.7) becomes

$$R'' + 2(R'^2+1)\left(\frac{R'}{r} + \frac{(rR'-R)((r^2+R^2)^2+3)}{(r^2+R^2)((r^2+R^2)^4-1)}\right) = 0\,, \tag{2.10}$$

where prime denotes a derivative with respect to r. We obtain a one-parameter family of Minkowski embedding solutions by integrating (2.10) using the initial values $R(0) = R_0 > 1$ and $R'(0) = 0$. The initial condition on R' comes from requiring the field equation to be non-singular at $r = 0$.

Figure 1 shows two D5-brane profiles. One is a Minkowski embedding that ends at $r = 0$ with $R_0 > 1$, while the other is a black hole embedding that extends to the horizon at $\upsilon = 1$. From the figure it is clear that there exists a borderline solution that belongs to both embedding classes. It can either be viewed as a black hole embedding solution with $\chi_0 = 1$ that enters the horizon at a vanishing angle, or equivalently as a Minkowski embedding solution with $R_0 = 1$ that caps off at the horizon.

Each D5-brane solution is characterised by two constants, m and c, that can be read off from the asymptotic behavior at the boundary,

$$\begin{aligned} \chi(\upsilon) &\sim \frac{m}{\upsilon} + \frac{c}{\upsilon^2} + \dots\,, \qquad \upsilon \to \infty\,, \qquad \text{BHE}\,, \\ R(r) &\sim m + \frac{c}{r} + \dots\,, \qquad r \to \infty\,, \qquad \text{ME}\,. \end{aligned} \tag{2.11}$$

They represent the boundary mass M_b and the condensate $\langle \mathcal{O}_b \rangle$ of $\mathrm{U}(1)_B$ flavour charged degrees of freedom in the dual field theory [20, 21, 22],

$$M_b = \frac{u_0}{2\sqrt{2}\pi\ell_s^2} m\,, \qquad \langle \mathcal{O}_b \rangle = -\frac{(4\pi\ell_s)^2}{\sqrt{2}}\, T_5\, u_0^2\, c\,. \tag{2.12}$$

Note that our definition of the boundary mass M_b differs from that in [1] by a factor of $\frac{\sqrt{\lambda}}{2\pi}$. By using (2.2) and (A.2), we see that the mass parameter m read off from our numerical solutions is proportional to the scale invariant ratio of the boundary mass and the temperature,

$$m = \frac{2\sqrt{2}}{\sqrt{\lambda}}\, \frac{M_b}{T} \equiv \frac{\bar{M}}{T}\,. \tag{2.13}$$

In the following, we will use m as a measure of the (inverse) temperature at fixed $\bar{M}$. Note that the trivial constant profile, $\chi(\upsilon) = 0$ ($\psi = \pi/2$), is a solution of the field equation (2.7) at any temperature and corresponds to $m = 0$.

In order to determine the thermodynamically stable D5-brane solution at a given temperature, we compare the regularised free energy of the different solutions. We review the main points of the regularisation procedure worked out in [23] in Appendix B and the resulting free energies are shown in Figure 2. The low-temperature phase, *i.e.* low $T/\bar{M}$, corresponds to a Minkowski embedding (or "gapped") solution, where the two-sphere shrinks down at a finite distance away from the horizon ($R(0) > 1$) and the spectrum of "quark-antiquark" bound states has a mass gap [20, 21, 24]. At high $T/\bar{M}$ the D5-tension can no longer balance the gravitational attraction of the background D3-branes and the favored solution is a black hole embedding solution, dual to a gapless

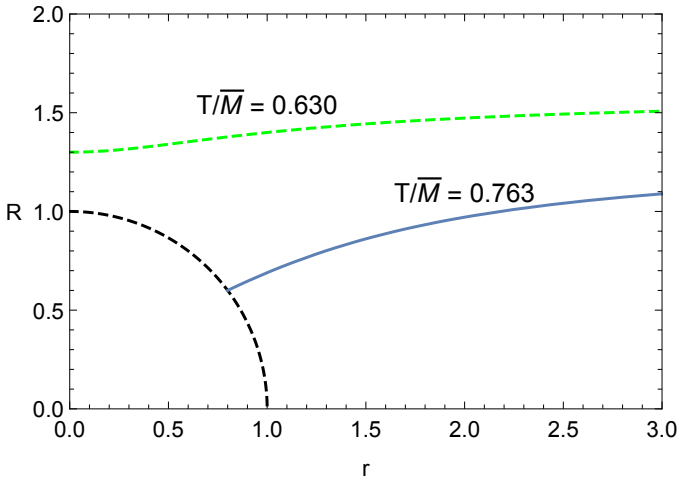

Figure 1: The embedding angle for the "Minkowski embedding" solution (dashed green curve) and the "black-hole embedding" solution (solid blue curve). The dashed black curve is the horizon at $v = 1$.

meson spectrum in the boundary field theory. There is a phase transition between the two types of embeddings. The right-hand plot in Figure 2 zooms in on the region near the critical temperature and reveals the characteristic swallow tail of a first-order transition. This is a universal feature of all Dp-Dq systems [20, 21].

The free energy shown in Figure 2 is obtained from numerical solutions of the field equations (2.7) and (2.10) at different temperatures. In Appendix D we consider its high and low temperature limits, where the field equations simplify and analytic results can be obtained.

2.2 Monopole two-point function

In order to calculate the two-point correlation function of monopole operators in the dual field theory we consider a probe D3-brane on top of the background D3-D5-brane system. The probe D3-brane ends on the D5-brane and thus appears as a magnetically charged object in the D5 worldvolume [13]. Furthermore, the D3-brane is embedded in AdS_5-Schwarzschild $\times$ S^5 in such a way that it wraps the same $S^2 \subset S^5$ as the D5-brane does and extends along a one-dimensional curve in AdS_4-Schwarzschild $\subset$ AdS_5-Schwarzschild with endpoints at the AdS_4 boundary. This accounts for three out of four of the D3 worldvolume directions. The remaining worldvolume direction is transverse to the D5-brane, along ψ in the parametrisation (2.1), from $\psi = 0$ to $\psi(u)$ where the D3-brane ends on the D5-brane. The probe D3-brane thus appears as a particle in AdS_4-Schwarzschild and is magnetically charged under the D5 world-volume gauge field A, *i.e.* it models a bulk magnetic monopole [1].

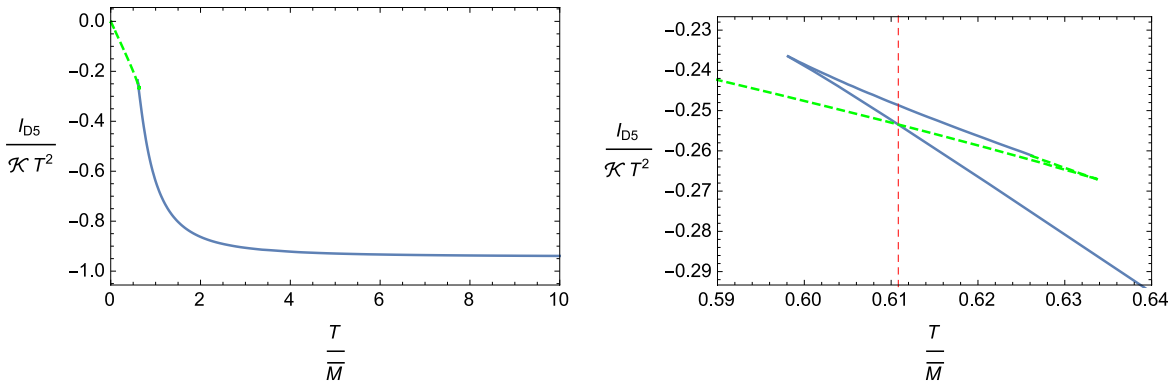

Figure 2: Regularised free energy for a D5-brane in D3-branes background. The dashed green (solid blue) curves correspond to Minkowski (black hole) embeddings. The figure on the right shows an expanded view of the region near the phase transition. The dotted vertical red line indicates the critical temperature $T_c/\bar{M} = 0.611$.

The D3-brane fills part of the $S^3 \subset S^5$ described by (ψ, θ, ϕ) in (2.1). The fraction of the S^3 volume that is filled depends on the D5 embedding. At the boundary, the D5-brane is at $\psi = \frac{\pi}{2}$ and the D3-brane fills half of the S^3. The curve connecting the insertion points on the AdS_4 boundary extends into the AdS_4-Schwarzschild bulk, where the D5-brane generically moves away from $\psi = \frac{\pi}{2}$ and the D3-brane occupies a smaller fraction of the S^3 volume. In particular, if the curve extends to where the D5-brane caps off in a Minkowski embedding then the volume of the D3-brane shrinks to zero at that point.

Computing the two-point boundary monopole correlation function in the large N-limit amounts to evaluating the corresponding on-shell D3-brane action as a function of the separation between the brane endpoints on the AdS_4 boundary. In Section 3 we present results from a numerical evaluation of the equal time two-point monopole correlator at finite temperature and background charge density, generalising the zero-temperature results obtained in [1]. We begin, however, with the simpler case of vanishing charge density at finite temperature.

We find it convenient to use D3-brane world-volume coordinates (s, χ, θ, ϕ) that match the coordinates we used for the D5-brane embedding in Section 2.1. Here s parametrises the curve $\{v(s), x(s), y(s)\}$ traced out by the probe D3-brane in the AdS_4-Schwarzschild part of the background geometry (2.4). This curve is spacelike when we consider a two-point function of monopole operators inserted at equal time on the boundary.[5] The variable $\chi = \cos\psi$ is restricted to the range $\chi_{D5} \leq \chi \leq 1$, where $\chi_{D5} = \chi\big(v(s)\big)$ corresponds to the intersection between the D5- and D3-brane worldvolumes.

[5]In this case the probe D3-brane is strictly speaking a D3-instanton.

In the charge neutral case, the action (A.20) for a probe D3-brane only contains the DBI term. Upon integrating over the coordinates (χ, θ, ϕ) the DBI action reduces to that of a point particle,

$$S_{D3} = N \int_{\mathcal{C}} \mathrm{d}s\, m_b(s) \sqrt{G_{xx}\left(\dot{x}(s)^2 + \dot{y}(s)^2\right) + G_{vv}\dot{v}(s)^2}, \tag{2.14}$$

where G_{IJ} is the pull-back of the ten-dimensional spacetime metric to the D3-brane world-volume, a dot indicates a derivative with respect to s, and $m_b(v)$ is a position dependent mass given by

$$m_b(v) \equiv \frac{\mu_b(v)}{L} \equiv \frac{2}{\pi L} \int_{\chi_{D5}}^{1} \sqrt{1-\chi^2}\, \mathrm{d}\chi\,. \tag{2.15}$$

We refer to the dimensionless quantity $\mu_b(v)$ as the effective mass of the bulk monopole.[6] It follows that the dynamics of the probe D3-brane depends on the embedding of the D5-brane it ends on. In a Minkowski embedding $\mu_b(v)$ shrinks to zero at the point where the D5 caps off, while in a black hole embedding $\mu_b(v)$ remains non-zero all the way to the horizon. This is clearly visible in Figure 3(a), which shows μ_b as a function of position at different temperatures.

For the actual computation, it is convenient to absorb the effective mass into the induced metric as a conformal factor and define a rescaled metric [1],

$$\tilde{G}_{IJ} = m_b^2(v)\, G_{IJ}\,. \tag{2.16}$$

The on-shell D3-brane action is then given by the length of a geodesic in the rescaled metric connecting the monopole operator insertion points at the AdS_4 boundary, which can without loss of generality be assumed to lie on the x-axis. The geodesic extends along $\{v(s), x(s)\}$ and intersects the boundary at $v \to \infty$, $x \to \pm\frac{\Delta x}{2}$. It has a turning point at $x = 0$, $v = v_*$, where $\frac{dv}{ds} = 0$.

As shown in Appendix C, the D3-brane action (2.14) can be re-expressed as

$$S_{D3} = 2N \int_{v_*}^{\infty} \mathrm{d}v \sqrt{\frac{\tilde{G}_{vv}}{1 - P^2 \tilde{G}^{xx}}} = 2N \int_{v_*}^{\infty} \mathrm{d}v \frac{\mu_b^2(v)}{\sqrt{v^2\mu_b^2(v) - 2\bar{P}^2 \tilde{f}^{-1}(v)}}\,, \tag{2.17}$$

where P is the conserved charge associated with translation invariance along the spatial x-direction, and $\bar{P}$ is the corresponding dimensionless variable,

$$P \equiv \dot{x}\, \tilde{G}_{xx}\,, \qquad \bar{P} = \frac{P}{\pi T}\,.$$

The separation of the D3 endpoints at the boundary is given by

$$\Delta x = 2 \int_{v_*}^{\infty} \sqrt{\frac{\tilde{G}_{vv}}{1 - P^2 \tilde{G}^{xx}}}\, \tilde{G}^{xx}\, P\, \mathrm{d}v\,, \tag{2.18}$$

[6] Note that our normalisation convention for μ_b differs from that of [1] by a factor of N.

which can in turn be expressed in terms of dimensionless quantities as

$$\Delta x\, \bar{M} = \frac{4m}{\pi} \int_{\upsilon_*}^{\infty} \frac{\mathrm{d}\upsilon}{\upsilon^2 \tilde{f}(\upsilon)} \frac{\bar{P}}{\sqrt{\upsilon^2 \mu_b^2(\upsilon) - 2\bar{P}^2 \tilde{f}^{-1}(\upsilon)}}\,. \tag{2.19}$$

In our numerical computation, $\bar{P}$ is an input parameter and we evaluate both the D3-brane action and the endpoint separation as a function of $\bar{P}$ for a given D5-brane embedding solution.

The location of the turning point, $\upsilon = \upsilon_*$ of a geodesic with $\bar{P} \neq 0$ depends on the D5-brane embedding. The condition for having a turning point is

$$\tilde{G}_{xx}(\upsilon_*) = P^2\,, \tag{2.20}$$

or equivalently

$$\upsilon_* = \sqrt{\frac{\bar{P}^2}{\mu_b^2(\upsilon_*)} + \sqrt{\frac{\bar{P}^4}{\mu_b^4(\upsilon_*)} - 1}}\,. \tag{2.21}$$

A real valued solution requires $|\bar{P}| \geq \mu_b(\upsilon_*)$. In a Minkowski embedding, this condition is always satisfied for some value of υ_* on the D5-brane because $\mu_b(\upsilon)$ goes to zero as the D5-brane caps off. In addition to geodesics with turning points, the Minkowski embedding supports a $\bar{P} = 0$ geodesic that extends "vertically" from the boundary to the point where the D5-brane caps off, depending on the type of D5-brane embedding. A pair of such vertical D3-branes turns out to be the thermodynamically favoured configuration at sufficiently large endpoint separation when the probe D5-brane is in a Minkowski embedding.

In a black hole embedding, on the other hand, the geodesic may reach the horizon at $\upsilon = 1$ before the turning point condition (2.21) is satisfied. In this case, the geodesic instead turns around at the horizon. This is not immediately apparent in the υ coordinate, because the coordinate transformation (2.3) is degenerate at the horizon, but by going back to the original u coordinate it is straightforward to show that the geodesic is quadratic in x near the horizon,

$$\frac{u(x)}{u_0} = 1 + \Big(\frac{\mu_{b,\mathrm{h}}^2}{\bar{P}^2} - 1\Big)\frac{u_0^2 x^2}{L^4} + O(x^4), \tag{2.22}$$

when $|\bar{P}| < \mu_{b,\mathrm{h}}$, where $\mu_{b,\mathrm{h}}$ is $\mu_b(\upsilon)$ evaluated at the horizon $\upsilon = 1$. This behaviour is also apparent in numerical solutions of the geodesic equation at sufficiently low $\bar{P}$.

The D3-brane action S_{D3} is in fact divergent for all the geodesic curves we have described. The divergence comes from the region near the boundary $\upsilon \to \infty$. We regularise it by introducing an upper cut-off at $\upsilon = \upsilon_{max} \gg 1$ in (2.17) and subtracting the action of a geodesic in the $\bar{P} \to 0$ limit,

$$S_{D3}^0 = 2N \int_{\upsilon_{min}}^{\upsilon_{max}} \mathrm{d}\upsilon \sqrt{\tilde{G}_{\upsilon\upsilon}} = 2N \int_{\upsilon_{min}}^{\upsilon_{max}} \mathrm{d}\upsilon\, \frac{\mu_b(\upsilon)}{\upsilon}\,, \tag{2.23}$$

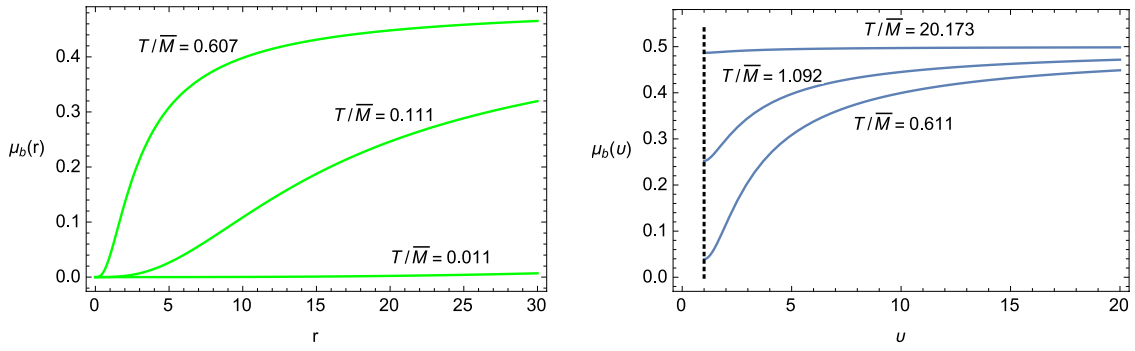

(a) Bulk monopole effective mass

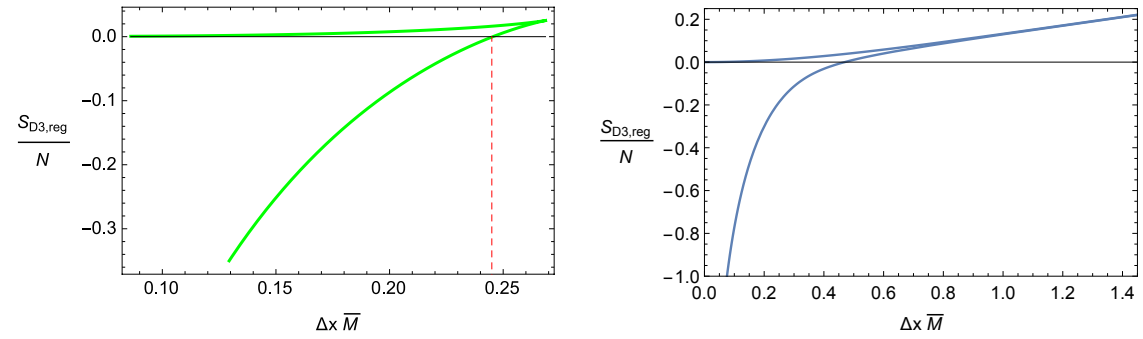

(b) Regularised D3-brane action

Figure 3: (a) Bulk monopole effective mass for Minkowski (black hole) embeddings on the left (right) at different temperatures; (b) Regularised D3-brane action versus Δx for Minkowski (black hole) embeddings on the left (right) at $T/\bar{M} = 0.1\,(0.68)$. The dashed vertical line in the left panel indicates the critical endpoint separation marking the transition from a single "hanging" geodesic to two disconnected vertical geodesics in a Minkowski embedding.

where υ_{min} depends on the D5-brane embedding. For a black hole embedding it is at the horizon, $\upsilon_{min} = 1$, while for a Minkowski embedding it is where the D5-brane caps off. In this case, we can use the coordinates $\{r\,, R\}$ introduced in (2.9) and set the lower limit of the radial variable in the integral to $r_{min} = 0$. By this convention, a disconnected configuration in Minkowski embedding, where two separate vertical D3-branes extend from the boundary, has vanishing regularised action.

In Figure 3(b) we plot the regularised action,

$$S_{D3,\text{reg}} \equiv S_{D3} - S^0_{D3}\,, \tag{2.24}$$

obtained by numerically evaluating the integrals in (2.17) and (2.23) for different values of the dimensionless parameter $\bar{P}$, against the endpoint separation Δx obtained at the same value of $\bar{P}$. For a Minkowski embedding the system undergoes a first order phase transition, similar to the zero-temperature case studied in [1], at a critical value of the endpoint separation, indicated by a dashed vertical line in the figure. At small values of the endpoint separation Δx, the thermodynamically stable branch consists of connected solutions with large $|\bar{P}|$, for which the turning point is located far from the cap of the D5-brane. Following this branch towards smaller $|\bar{P}|$, the turning point moves deeper into the bulk geometry while both the endpoint separation Δx and the regularised free energy (2.24) increase. Eventually the free energy becomes positive and this branch is disfavoured compared to a disconnected branch with two separate vertical D3-branes. The critical endpoint separation is indicated by a dashed vertical line in the figure.

Following the (now unstable) connected branch to smaller $|\bar{P}|$, the endpoint separation Δx increases towards a local maximum, which marks the endpoint of this branch of solutions. Even smaller values of $|\bar{P}|$ give rise to a third branch of solutions where the endpoint separation decreases from its local maximum and eventually approaches zero in the limit of vanishing $|\bar{P}|$. On this branch the turning point continues to move deeper into the bulk as $|\bar{P}|$ is decreased and touches the cap of the D5-brane precisely when $|\bar{P}| = 0$. The small $|\bar{P}|$ branch of solutions is always disfavoured compared to the other two branches. This is apparent from our numerical results but can also be seen by expanding the integrands in (2.17) and (2.19) in powers of $\bar{P}$ for very low $\bar{P}$. The endpoint separation is a linear function of $\bar{P}$, while the regularised action is a quadratic function of $\bar{P}$, and thus of Δx. It follows that the regularised action is always positive on this branch.[7]

For a black hole embedding the story is rather different. In this case the turning point of a "hanging" geodesic can be either outside the black hole or exactly at the horizon $\upsilon = 1$. The two possibilities give rise to two branches of D3-brane solutions and the branch that is thermodynamically stable at all values of the endpoint separation Δx

[7]Such a low momentum expansion is explicitly carried out for the more general case with non-zero background charge density in Appendix D.2.2.

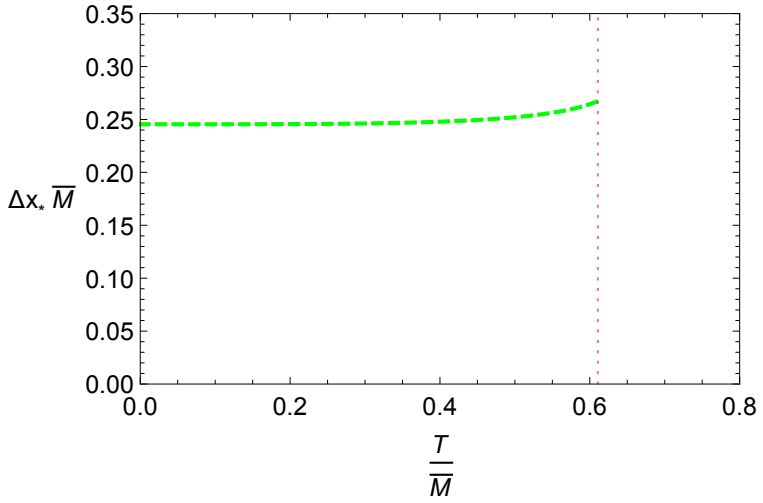

Figure 4: Temperature dependence of Δx_*, the critical separation between D3-brane endpoints in a Minkowski embedding, beyond which the thermodynamically favoured configuration consists of two separate segments extending vertically to where the D5-brane caps off. Above the critical temperature $T_c/\bar{M} = 0.611$ (indicated by the dotted vertical line) the D5 brane is in a black hole embedding where there is no disconnected D3-brane configuration.

turns out to be the one where the turning point is outside the horizon.[8]

The right panel in Figure 3(b) shows our numerical results for the regularised D3-brane action as a function of the endpoint separation in a black hole embedding. Following the stable branch towards larger Δx one finds a critical value of the conserved charge $|\bar{P}| = \mu_{b,\mathrm{h}}$ for which the geodesic touches the horizon at the turning point. At the critical value of $|\bar{P}|$ the $O(x^2)$ term in (2.22) vanishes. The unstable branch corresponds to $|\bar{P}|$ below the critical value and geodesics that turn around at the horizon.

Both the stable and unstable branches extend to infinite endpoint separation. To see this, consider the integrals in (2.17) and (2.19) precisely at the critical value $|\bar{P}| = \mu_{b,\mathrm{h}}$. It is straightforward to establish that both integrals diverge logarithmically in this case, with the divergence coming from the low end of the v integration, near the horizon. The divergence can, for instance, be regulated by introducing a cutoff at $v = 1 + \epsilon$ and

[8]In a black hole embedding there is no analog of the disconnected branch, with separate D3-brane segments extending from the boundary to where the D5-brane caps off, that dominates at large endpoint separation in a Minkowski embedding. If a D3-brane were to end at the horizon its boundary would include an S^2 of finite area that is not inside the D5-brane world-volume. We thank N. Iqbal for pointing out an error in a previous version of the paper concerning this issue.

in the limit of $\epsilon \ll 1$ one easily finds that[9]

$$\frac{S_{D3,\mathrm{reg}}}{N} \approx \pi T \mu_{b,\mathrm{h}} \Delta x \xrightarrow{T\to\infty} \frac{\pi}{2} T \Delta x. \tag{2.25}$$

The monopole two-point function (1.1) at high temperature is thus exponentially suppressed at large spatial separation with a characteristic length scale that scales inversely with temperature. This is the expected behaviour of a thermally screened system. At low temperatures, on the other hand, the D5-brane is in a Minkowski embedding and the favoured D3-brane configuration at large endpoint separation is a pair of disconnected vertical segments, for which the monopole two-point function is a constant independent of Δx. This signals the condensation of monopoles at low temperatures in this system. The critical endpoint separation, at which the disconnected configuration becomes dominant in the low-temperature Minkowski embedding phase, has a weak temperature dependence shown in Figure 4.

3 Finite charge density phase

3.1 Thermodynamics of charged D5-branes

By turning on a U(1) gauge field on the D5-brane we can generalise the results of the previous section to study monopole correlation functions in a compressible Fermi-liquid phase at finite charge density. We begin by giving a quick overview of the resulting charged D5-brane thermodynamics before turning our attention to the monopole correlators. Our discussion of D5-brane thermodynamics parallels that of [22], which considered charged D7-branes in a D3-brane background.

The Euclidean action for D5-brane at finite charge density is worked out in Appendix A. For convenience, we repeat the final expression (A.9) here,

$$I_{D5} = \mathcal{K}\, T^2 \int \mathrm{d}\upsilon\, \upsilon^2\, f \sqrt{\tilde{f}(1-\chi^2)\,(1-\chi^2+\upsilon^2\dot{\chi}^2)} \sqrt{\frac{Q^2}{\tilde{f}^2\upsilon^4\,(1-\chi^2)^2}+1}\,. \tag{3.1}$$

The induced metric on the D5-brane is still parametrised as in (2.5) and the finite charge density enters via the dimensionless parameter Q in the action (see Appendix A for details). The field equation for χ, obtained by varying (3.1), can be solved numerically using the same methods as employed for the charge-neutral case in Section 2.1. In the absence of explicit bulk sources, electric field lines emanating from the AdS_4 boundary have nowhere to end if the D5-brane caps off before the horizon [22]. The Minkowski embedding solutions are therefore unphysical at finite charge density and the only consistent solutions are black hole embeddings.

[9] A detailed analysis of these divergences, including the more general case at non-vanishing charge density, is presented in Appendix D.2.1.

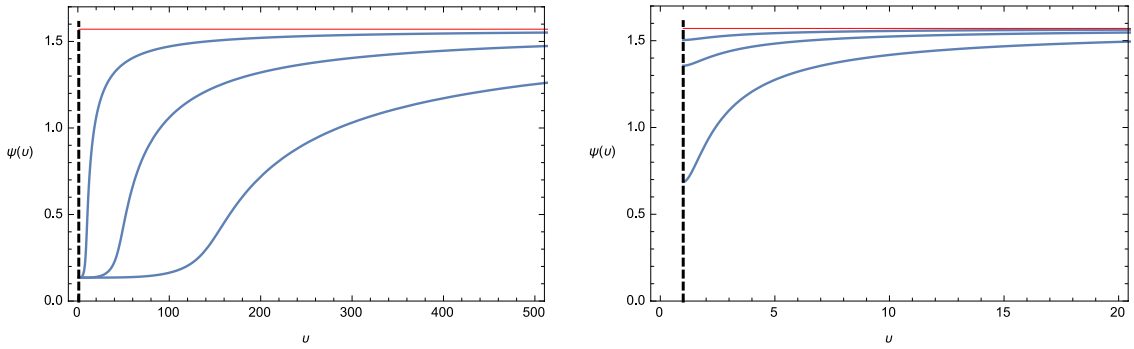

(a) Low temperature

(b) High temperature

Figure 5: D5-brane solutions at constant charge density $\bar{\rho} = 0.02$ for different temperatures. The red line represents constant embedding while the blue lines describe the BH embeddings for a) $T/\bar{M} = 0.1,\ 0.02,\ 0.006$ and b) $T/\bar{M} = 6.323,\ 2,\ 0.577$ from top to bottom. The dashed black line indicates the horizon at $\upsilon = 1$.

The relevant variables when it comes to the physical interpretation and presentation of our results are the temperature T and the charge density ρ in the boundary theory.[10] We fix the overall scale by working at a fixed boundary mass $\bar{M}$ and express our results in terms of dimensionless combinations,

$$m = \frac{\bar{M}}{T}\,, \qquad\qquad \bar{\rho} = \frac{\rho}{N\bar{M}^2}\,. \tag{3.2}$$

The phase diagram of the model is mapped out by separately varying $\bar{\rho}$ and m. In particular, if we keep $\bar{\rho}$ fixed and consider very high temperature we expect thermal effects to swamp any effect of the charge density while in the limit of low temperature the finite charge density should dominate. This is readily apparent in our numerical results, but we also demonstrate it explicitly by considering the different asymptotic limits of parameters in Appendix D.

Numerical solutions for χ are obtained by integrating the field equation outwards from the horizon, with the charge density Q and the boundary value at the horizon $\chi_0 = \chi(1)$ as dimensionless input parameters. For given values of the input parameters in the range $0 \leq \chi_0 \leq 1$ and $Q \geq 0$, the inverse temperature $m(\chi_0, Q)$ can be read off from the asymptotic behaviour of the numerical solution as in (2.11). The charge density $\bar{\rho}(\chi_0, Q)$ is then easily determined using the relation $\bar{\rho}\, m^2 = Q/2$. This procedure uniquely determines the physical variables m and $\bar{\rho}$ as functions of the numerical input parameters χ_0 and Q. The inverse mapping $(m, \bar{\rho}) \to (\chi_0, Q)$ is not single valued, however, and this leads to phase transitions as was already seen in the zero-charge case

[10]The physical charge density ρ is related to the temperature and the dimensionless parameter Q appearing in the action through (A.6).

in Section 2.1. The constant $\chi = 0$ solution is also present and can be viewed as the high-temperature limit of a black hole embedding, as is apparent in Figure 5.

In order to decipher the phase diagram, we compare the on-shell free energy density (3.1) on different branches of solutions. The UV divergence encountered as the D5-brane approaches the AdS boundary is regulated by introducing boundary counter-terms, as outlined in Appendix B. Numerical results for the regularised D5-brane free energy are shown in Figure 6(a) for different values of $\bar{\rho}$. At low charge densities, $\bar{\rho} < \bar{\rho}_* = 0.0145$, we find a first order phase transition between two branches of black hole embedding solutions. The left- and right-hand panels in Figure 6(b) showcase the different behaviour of the D5-brane free energy at $\bar{\rho} < \bar{\rho}_*$ and $\bar{\rho} > \bar{\rho}_*$, respectively. Figure 6(c) plots $\bar{\rho}$ against the critical temperature of the phase transition and shows how the critical line in the $T - \bar{\rho}$ plane terminates at $\bar{\rho} = \bar{\rho}_*$

The low-$\bar{\rho}$ phase transition connects to the phase transition between the black hole embedding and Minkowski embedding solutions at zero charge density. We note, in particular, that as $\bar{\rho} \to 0$ the critical temperature of the phase transition between the different black hole embedding branches approaches $T_c/\bar{M} = 0.611$, which is the critical temperature found in Section 2.1 at zero charge density. Furthermore, the stable black hole embedding solution at low temperature and low charge density approaches a Minkowski embedding solution. It almost caps off at a finite radial distance outside the black hole, leaving a narrow throat that extends all the way to the horizon to accommodate the electric field lines emanating from the black hole. In the $\bar{\rho} \to 0$ limit the throat degenerates and the solution takes the form of a Minkowski embedding solution. The onset of this low-temperature behaviour can be seen on the left in Figure 5 even if the D5-brane profiles in the figure are for a $\bar{\rho}$ value somewhat above ρ_*.

A similar phase diagram, involving charged D7-branes in the finite temperature background of a black 3-brane, was worked out in [22]. There it was argued that the favoured low-temperature configuration at charge densities below the analog of $\bar{\rho}_*$ in the D7-brane system may in fact be unstable. In the present paper we are mainly concerned with evaluating two-point correlation functions of monopole operators in the presence of the probe D5-brane and how they depend on the transverse spatial separation between the monopole insertions on the boundary. As it turns out, we can determine this spatial dependence without having to rely on D5-brane solutions at very low $\bar{\rho}$. In what follows, we therefore restrict our attention to charged D5-branes with $\bar{\rho} > \bar{\rho}_*$, where there is only one branch of solutions and the question of an instability, analogous to the one discussed in [22], does not arise.

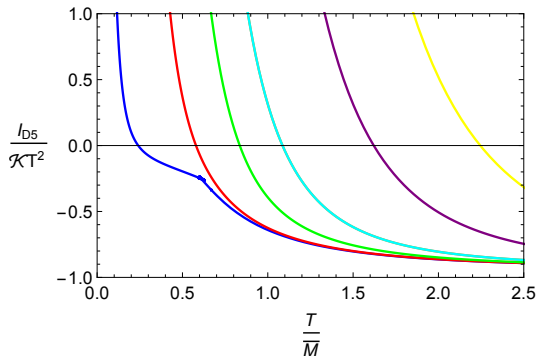

(a)

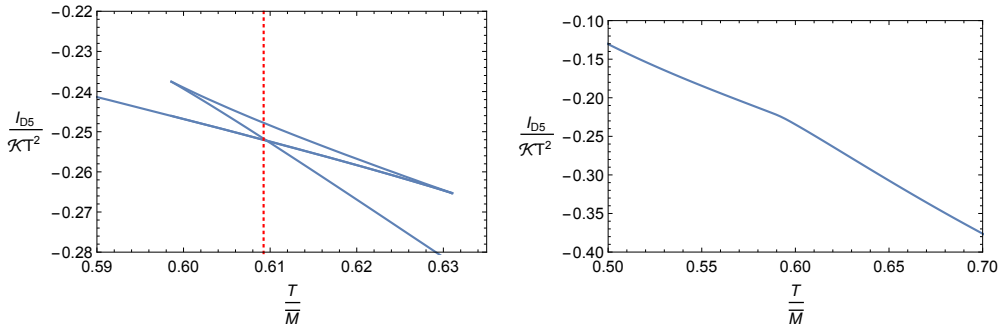

(b)

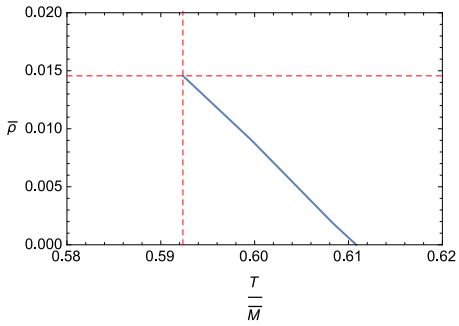

(c)

Figure 6: (a) Regularised free energy of charged D5-branes with $\bar{\rho} = 0.001, 0.1, 0.4, 0.8, 2, 4$ (from left to right). (b) Left panel: A close-up of the phase transition at low charge density ($\bar{\rho} = 0.001$). Right panel: Phase transition is absent at high charge density ($\bar{\rho} = 0.015$). (c) Charge density *vs.* critical temperature of phase transition at $\bar{\rho} < \bar{\rho}_* = 0.0145$.

3.2 Monopole two-point function at finite charge density

We now proceed to compute the action of a probe D3-brane ending on the charged D5-brane, which, under holographic duality, determines the two-point correlation function of monopole operators in a compressible finite charge density phase of the 2+1-dimensional defect field theory [1]. The calculation is a straightforward generalisation from the charge-neutral case that was presented in Section 2.2. The main new ingredient is the magnetic coupling between the probe D3-brane and the non-vanishing gauge field on the D5-brane world-volume. This means that the second term in the D3-brane action (A.20) in Appendix A comes into play and the spacelike curve $\mathcal{C}$ traced out by the probe D3-brane in the AdS_4-Schwarzschild part of the bulk geometry is no longer a geodesic in the rescaled metric (2.16). The endpoints at the AdS_4 boundary can still be taken to be at $\upsilon \to \infty$, $x \to \pm\frac{\Delta x}{2}$, $y \to 0$, but at intermediate points the curve extends in the y-direction and lies along $\{\upsilon(\eta), x(\eta), y(\eta)\}$. We refer the reader to Appendix C for the derivation of the shape of $\mathcal{C}$ and the regularised on-shell action of the probe D3-brane at finite charge density. The main focus of the present section will instead be on presenting our numerical results and exploring the behaviour of the monopole equal-time two-point function as a function of spatial separation at different temperatures and charge densities.

The Euclidean action of a D3-brane ending on a charged D5-brane is worked out in Appendix C below and is given by

$$S_{D3} = 2N \int_{\upsilon_*}^{\infty} \mathrm{d}\upsilon \, \frac{\mu_b^2(\upsilon)}{\sqrt{\upsilon^2 \mu_b^2(\upsilon) - 2\bar{\mathcal{P}}^2 \tilde{f}^{-1}(\upsilon)}} - \frac{\pi N \bar{\mathcal{P}}^2}{Q} \big(\omega\eta_e - \frac{1}{2}\sinh\left(2\omega\eta_e\right)\big) \,. \quad (3.3)$$

where

$$\omega\eta_e = \frac{2Q}{\pi} \int_{\upsilon_*}^{\infty} \mathrm{d}\upsilon \, \frac{1}{\upsilon^2 \tilde{f}(\upsilon) \sqrt{\upsilon^2 \mu_b^2(\upsilon) - 2\bar{\mathcal{P}}^2 \tilde{f}^{-1}(\upsilon)}} \,. \quad (3.4)$$

and $\eta \to \pm\eta_e$ at the endpoints of $\mathcal{C}$ at the AdS_4 boundary. The frequency ω, defined in (C.3), is the analog of a cyclotron frequency for a magnetic monopole in a background electric field. The curve has a turning point at $\eta = 0$ at the radial coordinate $\upsilon = \upsilon_*$. The dimensionless constant of integration $\bar{\mathcal{P}}$ is a measure of transverse momentum in the x-direction. It plays the same role as the parameter $\bar{P}$ in Section 2.2 and it is straightforward to see that $\bar{\mathcal{P}} \to \bar{P}$ as $Q \to 0$ (see Appendix C for details). In fact, the turning point analysis for a D3-brane ending on a D5-brane with a black hole embedding goes through unchanged, with $\bar{P}$ replaced by $\bar{\mathcal{P}}$. When $\bar{\mathcal{P}} > \mu_{b,\mathrm{h}}$, the curve $\mathcal{C}$ turns around at some $\upsilon = \upsilon_* > 1$ outside the horizon and returns to the boundary. On the other hand, for any $\bar{\mathcal{P}} \leq \mu_{b,\mathrm{h}}$, the curve turns around at the horizon.

The first term in (3.3) comes from the geometric DBI-action of the D3-brane and reduces to (2.17) for the uncharged case. The second term, which arises from the

magnetic coupling between the probe D3- and D5-branes, vanishes in the $Q \to 0$ limit. A regularised D3-brane action is obtained as before, by subtracting the action (2.23) of a $\bar{\mathcal{P}} = 0$ curve. This cancels the divergence coming from the near boundary region $\upsilon \to \infty$.

In order to determine how the monopole two-point function behaves as a function of the endpoint separation, we plot the result of a numerical evaluation of the regularised action against Δx for different values of $\bar{\mathcal{P}}$ at fixed temperature and charge density. In Appendix C we obtain the following expression for the endpoint separation in terms of dimensionless input parameters,

$$\Delta x \bar{M} = \frac{2m\bar{\mathcal{P}}}{Q} \sinh\left(\omega \eta_e\right) , \tag{3.5}$$

which can easily be evaluated numerically.

The graphs in figure 7 show our results for the regularised D3-brane action as a function of Δx for several temperatures at two values of the charge density: $\bar{\rho} = 0.02$ in Figure 7(a) and $\bar{\rho} = 10$ in Figure 7(b). At low charge density ($\bar{\rho} \lesssim 0.1$) and low temperature ($T \lesssim 0.6\bar{M}$ at $\bar{\rho} = 0.02$) we see evidence for a first-order transition between two D3-branes that have different values of $\bar{\mathcal{P}}$. Both have $\bar{\mathcal{P}} > \mu_{b,\mathrm{h}}$ and thus the turning point is outside the horizon on both branches.[11] In the limit of vanishing charge density, this transition reduces to the transition between connected and disconnected D3-brane configurations that we saw for D5-branes in Minkowski embedding in the charge-neutral case in Section 2.2. This is evident in Figure 8, which plots the critical endpoint separation Δx^* as a function of temperature at low charge density ($\bar{\rho} = 0.02$) and compares it to that of the connected-disconnected transition.

The graphs showing the regularised action of a connected D3-brane in Figure 7 share a common feature in that they all become convex at sufficiently large Δx. This can be traced to the magnetic term being dominant over the geometric DBI term in (3.3) at large endpoint separation while the DBI term governs the short-distance behaviour. A detailed analysis carried out in Appendix D.2.1 shows that the regularised D3-brane action always depends quadratically on Δx in the "magnetic regime" at sufficiently large Δx. This, in turn, leads to Gaussian suppression of the equal-time two-point correlation function of monopole operators as a function of the distance between the operator insertion points on the boundary.

The significance of the Gaussian suppression depends, however, on the value of the charge density in relation to the temperature. At high $\bar{\rho}$ or low $T/\bar{M}$ the Gaussian behaviour sets in at relatively short distances, as can for instance be seen in Figure 7(b). This matches the zero temperature results of [1] where the monopole two-point function

[11] As in the charge-neutral case, there is also a branch with $\bar{\mathcal{P}} < \mu_{b,\mathrm{h}}$ and a turning point on the horizon itself but this branch is never the most stable one. It is indicated with dashed lines in some of the graphs in Figure 7 but is left out of the others to avoid clutter.

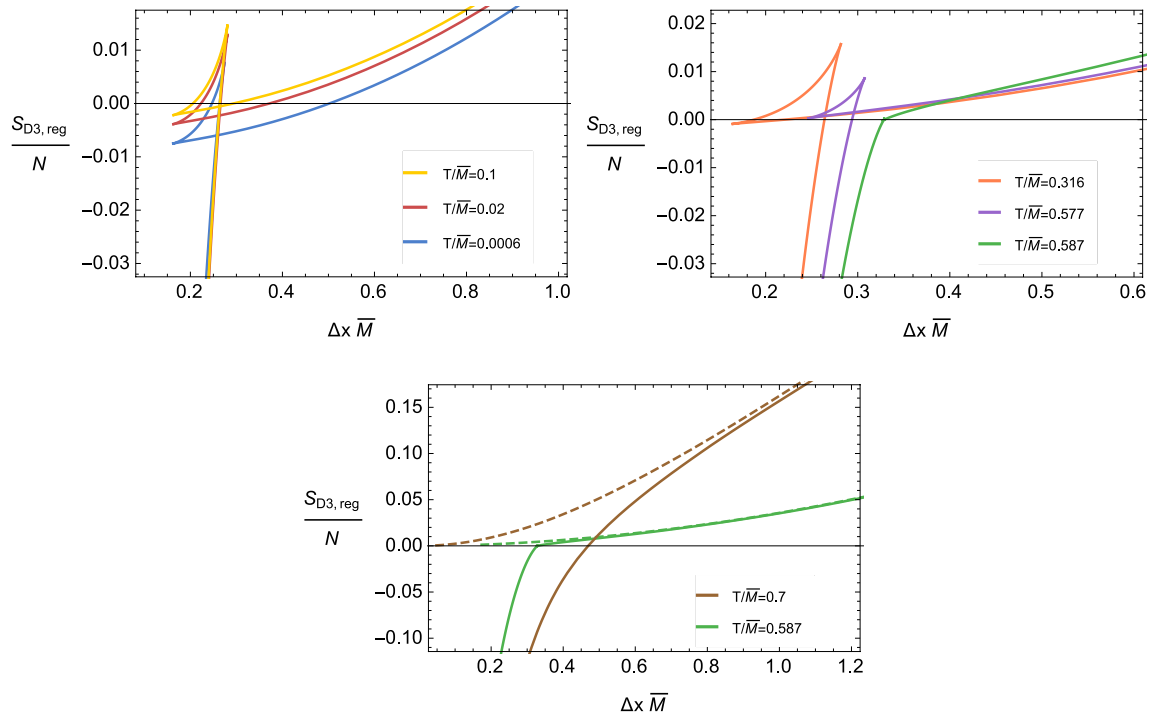

(a) $\bar{\rho} = 0.02$

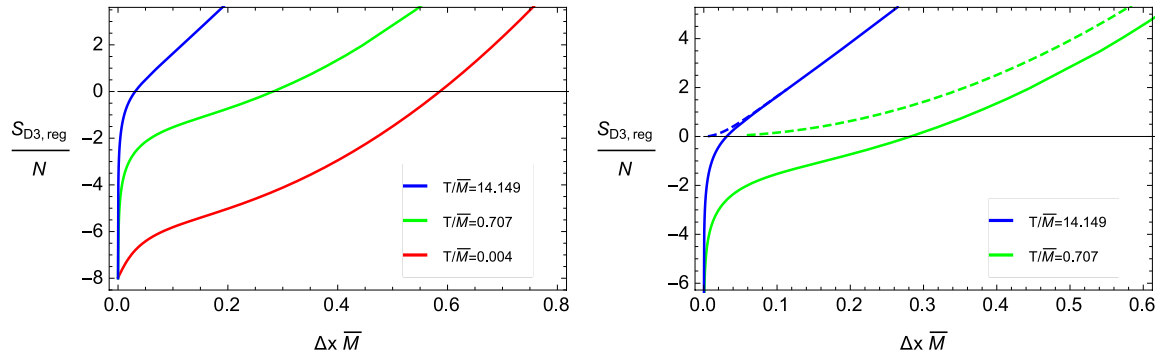

(b) $\bar{\rho} = 10$

Figure 7: Euclidean D3-brane action against $\Delta x \bar{M}$ at (a) $\bar{\rho} = 0.02$ and (b) $\bar{\rho} = 10$. Each curve corresponds to a given temperature as indicated. The unstable $\bar{\mathcal{P}} < \mu_{b,\mathrm{h}}$ branch is indicated by dashed lines in the middle and bottom right plots, but omitted from the others to avoid clutter.

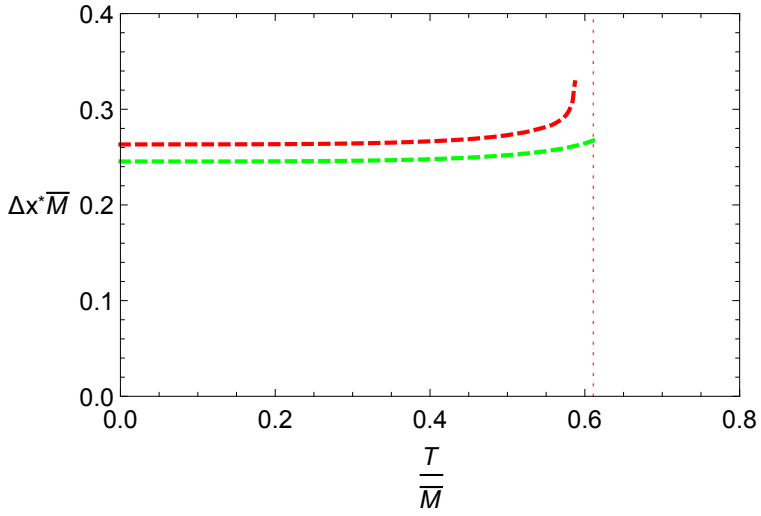

Figure 8: The dashed red curve shows the critical endpoint separation Δx^* for the first-order transition between two branches of solutions, at $\bar{\rho} = 0.02$ as a function of temperature. The dashed green curve (repeated from Figure 4 for reference) shows the endpoint separation at which the disconnected branch of D3-brane solutions becomes thermodynamically favoured in a Minkowski embedding at $\bar{\rho} = 0$.

was found to be Gaussian suppressed with distance at finite charge density. At low $\bar{\rho}$ or high $T/\bar{M}$, on the other hand, the Gaussian behaviour only sets in at such long distances that the monopole two-point function is already vanishingly small due to the exponential suppression from thermal screening discussed at the end of Section 2.2.

Our results for the monopole two-point function at finite $\bar{\rho}$ and T thus interpolate nicely between Gaussian suppression obtained when the charge density dominates over the temperature and exponential thermal screening found at low charge density.

4 Discussion

We have computed equal-time two-point correlation functions of magnetic monopole operators in a strongly coupled 2+1-dimensional U(1) gauge theory and studied their spatial dependence. This provides information about the phase structure of the theory, including possible monopole condensation in a phase with a charge gap, and also allows us to probe a compressible phase at finite U(1) charge density. Our investigation employs a top-down holographic construction involving intersecting D5- and D3-branes in $AdS_5 \times S^5$ spacetime, originally developed by Iqbal in [1], and extends it to an AdS_5-Schwarzschild $\times S^5$ black hole background in order to include thermal effects and explore monopole correlators across the $\rho - T$ phase diagram.

In Section 2 we focused on thermal effects on monopole correlators in a holographic phase with a charge gap at zero temperature. The analysis performed in [1] showed that in this phase the holographic monopole two-point function at zero temperature saturates to a constant value as the separation between the operator insertions is increased. This is the expected behaviour when the monopole operator has condensed. On the gravitational side of the holographic duality the condensation is attributed to the vanishing of the bulk monopole effective mass where the D5-brane, on which the D3-brane representing the bulk monopole ends, caps off in a Minkowski embedding. We find that the saturation of the monopole two-point function at long distances persists at finite temperature, up to the critical temperature where the D5-brane makes a transition from a Minkowski to a black hole embedding. Above the critical temperature, however, the monopole operator is no longer condensed and the two-point function is exponentially suppressed at long distances due to thermal screening.

In Section 3 we turned our attention to thermal effects in a compressible phase in the presence of a non-zero U(1) charge density implemented by introducing a gauge field on the D5-brane world-volume. On the one hand, the finite charge density forces the D5-brane into a black hole embedding at any non-zero temperature and on the other hand it gives rise to a direct coupling between the D3-brane and the magnetic dual of the world-volume gauge field on the D5-brane. Studying the monopole correlation function at finite temperature and charge density, we find that the transition to a disconnected D3-brane configuration at large separation found at vanishing charge density is replaced by a transition between different connected D3-brane configurations at low, but non-vanishing, charge densities and relatively low temperature.

We also observe effects of the interplay at finite temperature and charge density between the magnetic coupling and the geometric DBI-term in the D3-brane action. On the dual field theory side, this shows up in the dependence of the monopole operator two-point function on spatial distance. In particular, at finite charge density and low temperature the magnetic coupling contribution is the dominant one and the two-point function has a Gaussian falloff with distance. This is in line with the zero-temperature findings of [1]. At high temperature and low charge density, on the other hand, the monopole two-point function exhibits exponential falloff due to thermal screening, but eventually crosses over to Gaussian suppression at very long distances.

In this work we restricted our attention to the combined effects of finite charge density and temperature on two-point functions of monopole operators. An interesting and rather straightforward extension would be to add a non-zero magnetic field, for instance along the lines of [15]. Another future direction would be to relax some of the constraints that are built into the particular top-down holographic model used here in order to explore more general bulk monopole embeddings and the corresponding phase diagrams. Our treatment involved a probe D3-brane ending on a probe D5-brane in an

AdS_5-Schwarzschild $\times S^5$ background. An important question is whether including the back-reaction of the D3/D5-brane system on the background geometry would stabilise or wash out the features we have found. Modelling the back-reaction may require the added flexibility of a bottom-up approach, while retaining essential features of the top-down D-brane construction. At the same time, the study of monopole dynamics in phenomenologically motivated bottom-up models would be of considerable interest in its own right. Finally, there are other intersecting D-brane systems which can be used to model monopole operators in strongly coupled gauge theory. A D5/D7-brane model might for instance be a more natural setting to study non-Abelian monopole correlators.

Acknowledgements

We thank N. Evans, G. Grignani, N. Iqbal, N. Jokela, M. Lippert, R. Myers, A. Peet, S. Ross, and T. Zingg for helpful discussions. We thank J. Á. Thorbjarnarson and P. R. Bryde for useful comments. R.P. thanks the Perimeter Institute for Theoretical Physics for hospitality during the completion of this work. This research was supported in part by the Icelandic Research Fund under contracts 163419-051 and 163422-051, the Swedish Research Council under contract 621-2014-5838, and by grants from the University of Iceland Research Fund.

A Action functionals for probe D-branes

In this Appendix we collect some formulae and expressions which are used in the main body of the paper and in later appendices. We work out the explicit form of the D5-brane action in the coordinate system used in the main text. This is standard material but is included here in order to have a self-contained presentation. We also obtain an explicit expression for the probe D3-brane action of a bulk monopole proposed by Iqbal in [1] in a black 3-brane background.

The tension of a Dp-brane is given by

$$T_p = \frac{1}{(2\pi)^p g_s \, (\ell_s)^{p+1}} \,, \tag{A.1}$$

where g_s is the string coupling constant, and ℓ_s the string length, which in turn are related to the 't Hooft coupling constant λ, the AdS radius L, and the number of background D3-branes N as follows [25],

$$\ell_s^2 = \alpha' \,, \qquad g_s = \frac{\lambda}{4\pi N} \,, \qquad \frac{L}{\ell_s} = \lambda^{\frac{1}{4}} \,. \tag{A.2}$$

A.1 D5-brane

The world-volume action for the probe D5-brane is

$$S_{D5} = T_5 \int_{D5} 2\pi\alpha' F \wedge C_4 - T_5 \int_{D5} \mathrm{d}^6\sigma \, \sqrt{-\det\left(\gamma_{D5} + 2\pi\alpha' F\right)} \,. \tag{A.3}$$

where C_4 denotes the Ramond-Ramond 4-form field sourced by the background D3-branes, $F = dA$ the 2-form field strength of the D5-brane world-volume gauge field, and γ_{D5} the induced D5 world-volume metric. The first term in (A.3) vanishes for the D5-brane configuration investigated in this work. To see this, we choose a gauge where the 4-form C_4 is a sum of two terms, one proportional to the volume form on $\mathbb{R}^4 \subset \mathrm{AdS}_5$-Schwarzschild and the other to the volume form on the product of the two S^2 factors inside S^5. The former gives zero when wedged with the 2-form F while the latter has vanishing pullback to the D5-brane world-volume.

In order to evaluate the remaining DBI term in (A.3) we take γ_{D5} to be the induced metric in static gauge (2.5) and parametrise the U(1) gauge potential on the D5-brane world-volume as follows,

$$A_t(\upsilon) = \frac{\sqrt{\lambda}}{2\pi} a_t(\upsilon) \,. \tag{A.4}$$

After some straightforward algebra the D5-brane action reduces to

$$S_{D5} = -\frac{\sqrt{\lambda}}{4\pi} N V_3 T^2 \int \mathrm{d}\upsilon \left(1-\chi^2\right) \upsilon^2 \tilde{f} \sqrt{-\dot{a}_t^2 + \frac{\pi^2 \, T^2 \, f^2}{2\tilde{f}} \left(1 + \frac{\upsilon^2 \dot{\chi}^2}{1-\chi^2}\right)}, \tag{A.5}$$

where N is the number of background D3-branes, V_3 is the (infinite) volume from the integration over the t, x, y variables, T is the temperature of the background (2.2), and the dot denotes a derivative with respect to υ. Since the action (A.5) depends only on the derivative of the gauge potential a_t, it is convenient to introduce a charge density,

$$\rho = \frac{1}{V_3} \frac{2\pi}{\sqrt{\lambda}} \frac{\delta S_{D5}}{\delta \dot{a}_t} = \frac{1}{2} N \, T^2 \, Q \,, \tag{A.6}$$

with

$$Q \equiv \frac{\dot{a}_t \, \upsilon^2 \, \tilde{f} \, \left(1-\chi^2\right)}{\sqrt{-\dot{a}_t^2 + \frac{\pi^2 \, T^2 \, f^2}{2\tilde{f}} \left(1 + \frac{\upsilon^2 \dot{\chi}^2}{1-\chi^2}\right)}} \,. \tag{A.7}$$

The equation of motion of the gauge field implies radial conservation of the charge density,

$$\frac{d}{d\upsilon} Q = 0 \,. \tag{A.8}$$

We can take advantage of this by performing a Legendre transform on (A.5) that trades the gauge potential a_t for Q as the independent field variable. This leads to an action functional for χ that includes the conserved charge density Q as a parameter,

$$I_{D5} = \mathcal{K}\, T^2 \int \mathrm{d}\upsilon\, \upsilon^2\, f\, \sqrt{\tilde{f}(1-\chi^2)\,(1-\chi^2+\upsilon^2\dot{\chi}^2)}\sqrt{\frac{Q^2}{\tilde{f}^2\upsilon^4\,(1-\chi^2)^2}+1}\,. \tag{A.9}$$

In order to study D5-brane thermodynamics, we have changed to Euclidean signature and taken Euclidean time to be periodic with period $1/T$. The temperature dependence of the constant in front of the action is left explicit and

$$\mathcal{K} \equiv \frac{\sqrt{\lambda}\, N\, V_2}{4\sqrt{2}}\,, \tag{A.10}$$

with V_2 the transverse area coming from the integral over x and y.

The free energy of a D5-brane at charge density Q is given by the on-shell value of the Euclidean action (A.9). The boundary counter-terms needed to regularise the free energy are discussed in Appendix B and numerical results for the resulting regularised on-shell action are presented in Section 3.1. Switching off the charge density Q gives the free energy of a charge neutral D5-brane,

$$I_{D5} = \mathcal{K}\, T^2 \int \mathrm{d}\upsilon\, \upsilon^2\, f\, \sqrt{\tilde{f}(1-\chi^2)\,(1-\chi^2+\upsilon^2\dot{\chi}^2)}\,, \tag{A.11}$$

considered in Section (2.1).

A.2 D3-brane

The action for the probe D3-brane is

$$S_{D3} = T_3 \int_{D3} C_4 - T_3 \int_{D3} \mathrm{d}^4\sigma\, \sqrt{-\det\left(\gamma_{D3} + 2\pi\alpha' F_{(3)}\right)}\,, \tag{A.12}$$

where $F_{(3)}$ is the field strength of the D3-brane world-volume gauge field and γ_{D3} the induced D3-brane world-volume metric. Gauge invariance of (A.3) and (A.12) with respect to the C_4 gauge transformation,

$$\delta_\Lambda C_4 = d\Lambda_3\,, \tag{A.13}$$

requires the presence of additional terms,

$$S_K = \int_{D5} K_3 \wedge dF + q_m \int_{\partial D3} K_3\,, \tag{A.14}$$

involving a 3-form Lagrange multiplier K_3 that transforms as follows under the gauge transformation (A.13),

$$\delta_\Lambda K_3 = -2\pi\alpha' T_5 \Lambda_3\,. \tag{A.15}$$

Note that this fixes the value of the coupling constant q_m to be

$$q_m = \frac{T_3}{2\pi\,\alpha'\,T_5} = 2\pi\,. \tag{A.16}$$

The 3-form K_3 provides the magnetic coupling between the gauge field living on the D5-brane and the edge of the D3-brane. Indeed, adopting the same ansatz as in [1],

$$K_3 = \frac{1}{4\pi}\tilde{A}\wedge\omega_2\,, \tag{A.17}$$

with ω_2 the volume form on the two-dimensional unit sphere that the D5 and D3-branes wrap around inside S^5, the three-dimensional term in (A.14) reduces to an integral,

$$q_m\int_{\mathcal{C}}\tilde{A}\,, \tag{A.18}$$

along the curve $\mathcal{C}$ in AdS_4-Schwarzschild traced out by the probe D3-brane.

The field strength of $\tilde{A}$ is the magnetic dual of the field strength of the D5-brane world-volume gauge field A [1]. To see this, we vary the full action with respect to the field strength of A. Only two terms contribute, *i.e.* the DBI-term in (A.3) and the D5-brane world-volume term in (A.14). Using the definitions (A.6) and (A.17), we obtain the following rather simple result,

$$d\tilde{A} = \rho\,dx\wedge dy\,, \tag{A.19}$$

which is the magnetic dual of the radial electric field sourced by the charge density ρ. It follows that we can choose a gauge where $\tilde{A} = -\rho\,y\,dx$.

Finally, we collect the terms that contribute to the bulk monopole dynamics. Due to the specific D3-brane embedding employed in our analysis, the first term in (A.12) containing the Ramond-Ramond potential C_4 vanishes and the remaining DBI term simplifies because there is no gauge field on the D3-brane worldvolume. As explained in Section 2.2, for equal-time correlation functions the curve spanned in AdS_4-Schwarzschild by the probe D3-brane is spacelike and therefore the induced metric γ_3 has Euclidean signature. The relevant terms in the Euclidean D3-brane action are thus [1]

$$S_{D3} = T_3\int_{D3}\mathrm{d}^4\sigma\,\sqrt{\det\gamma_3} + i\,q_m\int_{\mathcal{C}}\tilde{A}\,. \tag{A.20}$$

In the charge-neutral case, considered in Section 2.2, the second term is absent and the DBI term reduces to the action for a point particle (2.14) with a mass that depends on the radial position in AdS_4-Schwarzschild. In this case, the on-shell D3-brane action is simply given by the length of a geodesic in a rescaled metric where the position dependent mass has been absorbed as a conformal factor, as discussed in Section 2.2. At finite charge density, on the other hand, the magnetic term in (A.20) is non-vanishing and the curve $\mathcal{C}$ will no longer be a geodesic in the rescaled metric. This case is considered in detail in Appendix C.

B Boundary counter-terms for D5-brane

In the main text, we encountered several branches of D5-brane solutions. When two or more different solutions exist for the same values of physical parameters it is important to identify which solution is thermodynamically stable. For this, we need to evaluate the free energy given by the on-shell Euclidean action of the D5-brane and compare between different branches of solutions. In the charge-neutral case this involves a comparison between Minkowski and black hole embedding solutions, while at finite charge density we compare the free energy of different branches of black hole embedding solutions.

As it stands, the D5-brane free energy (A.9) is UV-divergent and needs to be regularised by introducing appropriate counter-terms at the AdS_4 boundary. We use a well-established regularisation procedure for general Dp-Dq systems described by DBI actions [23] and specialise to the system at hand. We take the UV cut-off surface to be at constant radial coordinate $\upsilon = \upsilon_{UV}$ and find that the following counter-term action will cancel the UV-divergence of the bulk D5-brane action,

$$S_{\rm b} = -\frac{\sqrt{\lambda}N}{6\pi^3 L^3}\int {\rm d}^3\xi\sqrt{\gamma^{\rm b}}\left(1-\frac{3}{2}\chi^2+\ldots\right)\Big|_{\upsilon=\upsilon_{UV}}\,, \tag{B.1}$$

where $\xi^i = (\tau, x, y)$ are boundary coordinates and $\gamma^{\rm b}_{ij}$ the induced metric at $\upsilon = \upsilon_{UV}$. A finite free energy is obtained by cutting off the integral at $\upsilon = \upsilon_{UV}$ in (A.9), or in (A.11) in the charge-neutral case, and evaluating the sum

$$I_{D5,\rm reg} = I_{D5} + S_{\rm b} \tag{B.2}$$

before taking the $\upsilon_{UV} \to \infty$ limit. The ellipsis in (B.1) denotes sub-leading terms that give a vanishing contribution in the limit. We note that the presence of a gauge field on the D5-brane world-volume does not require any additional boundary counter-terms compared to the charge-neutral case.

The regularised free energy can now be calculated numerically as a function of temperature for both black hole and Minkowski embeddings.[12] Results are shown in Figure 2 for the charge-neutral case and in Figure 6 for D5-branes at finite charge density.

C On-shell D3-brane action

In this Appendix we generalise the discussion of monopole two-point functions in Section 2.2 to finite charge density. We obtain integral expressions for the on-shell D3-brane action and for the endpoint separation on the AdS_4 boundary, in terms of dimensionless parameters that characterise the background charge density ρ and the curve $\mathcal{C}$ in

[12] For efficient numerical evaluation of the free energy of a Minkowski embedding solution, it is convenient to change to the $(r\,, R)$ variables introduced in Section 2.1.

AdS_4 that connects the two endpoints. Results from the numerical evaluation of these expressions are presented and discussed in Section 3.2 of the main text.

Our starting point is the Euclidean D3-brane action (A.20). Using the D3-brane world-volume coordinates $(s, \upsilon, \theta, \phi)$ that were introduced in Section 2.2, the action reduces to

$$S_{D3} = N \int_{\mathcal{C}} \mathrm{d}s \sqrt{\tilde{G}_{xx}\big(\dot{x}(s)^2 + \dot{y}(s)^2\big) + \tilde{G}_{\upsilon\upsilon}\,\dot{\upsilon}(s)^2} - i\,q_m\,\rho \int_{\mathcal{C}} \mathrm{d}s\, y(s)\,\dot{x}(s)\,, \tag{C.1}$$

where $\tilde{G}_{IJ}$ are components of the rescaled metric (2.16) and a dot denotes a derivative with respect to s. The following Noether charges are conserved along the curve $\mathcal{C}$,

$$P_x = \tilde{G}_{xx}\,\dot{x} - i\,\omega\,y\,, \qquad P_y = \tilde{G}_{xx}\,\dot{y} + i\,\omega\,x\,, \tag{C.2}$$

where

$$\omega \equiv \frac{q_m\,\rho}{N} = \pi T^2 Q \tag{C.3}$$

is the analog of a cyclotron frequency for a magnetic monopole in an electric field, and we have simplified the expression for the charges by using the constraint

$$\tilde{G}_{xx}\big(\dot{y}(s)^2 + \dot{x}(s)^2\big) + \tilde{G}_{\upsilon\upsilon}\,\dot{\upsilon}(s)^2 = 1\,, \tag{C.4}$$

that follows if s is taken to be an affine parametrisation of $\mathcal{C}$.

The change of variables

$$\tilde{G}_{xx}\frac{d}{ds} = \frac{d}{d\eta} \tag{C.5}$$

allows us to re-express the charges as

$$P_x = x'(\eta) - i\omega\,y(\eta)\,, \qquad P_y = y'(\eta) + i\omega\,x(\eta)\,, \tag{C.6}$$

where prime denotes a derivative with respect to the new parameter η. We want to solve this system of first order differential equations subject to suitable boundary conditions. Without loss of generality, we can assume that the midpoint of the curve $\{\upsilon(\eta), x(\eta), y(\eta)\}$ is at $\eta = 0$ and the endpoints at $\eta = \pm\eta_e$. The following conditions,

$$x(0) = 0, \qquad x(\pm\eta_e) = \pm\frac{\Delta x}{2}, \qquad y(\pm\eta_e) = 0, \qquad \upsilon(\pm\eta_e) \to \infty, \tag{C.7}$$

then ensure that the curve intersects the boundary at $x \to \pm\frac{\Delta x}{2}$ and $y \to 0$. A simple solution of (C.6) satisfying these conditions is given by

$$x(\eta) = \beta \sinh(\omega\eta)\,, \qquad y(\eta) = i\beta\big(\cosh(\omega\eta_e) - \cosh(\omega\eta)\big) \tag{C.8}$$

where we have used translation symmetry in the x-direction to set $P_y = 0$ and the parameters β and η_e are determined by the remaining Noether charge and the endpoint separation through

$$P_x = \beta\omega \cosh(\omega\eta_e)\,, \qquad \Delta x = 2\beta \sinh(\omega\eta_e)\,. \tag{C.9}$$

By using (C.5), we can write the constraint (C.4) as

$$\tilde{G}^{xx}\omega^2\beta^2 + (\tilde{G}^{xx})^2\tilde{G}_{\upsilon\upsilon}\,\upsilon'(\eta)^2 = 1\,, \tag{C.10}$$

or equivalently

$$\Big(\frac{\mathrm{d}\eta}{\mathrm{d}\upsilon}\Big)^2 = \frac{(\tilde{G}^{xx})^2\tilde{G}_{\upsilon\upsilon}}{1-\omega^2\beta^2\tilde{G}^{xx}}\,. \tag{C.11}$$

The value of the dimensionless product $\omega\eta_e$ at the endpoint can then be obtained as an integral over the radial variable,

$$\omega\eta_e = \frac{2Q}{\pi}\int_{\upsilon_*}^{\infty}\mathrm{d}\upsilon\,\frac{1}{\upsilon^2\tilde{f}\sqrt{\upsilon^2\mu_b(\upsilon)^2 - 2\bar{\mathcal{P}}^2\tilde{f}^{-1}(\upsilon)}}\,, \tag{C.12}$$

where $\upsilon_* \equiv \upsilon(0)$ denotes the turning point of the curve $\mathcal{C}$ and

$$\bar{\mathcal{P}} \equiv \frac{\omega\beta}{\pi T} \tag{C.13}$$

is a dimensionless combination of input parameters. The D5-brane embedding enters through $\mu_b(\upsilon)$, the dimensionless effective mass of the bulk monopole defined in (2.15).

Similarly, the DBI-term in the D3-brane action (C.1) can be written as a radial integral while the magnetic term can be obtained in closed form in terms of the endpoint variable in (C.12),

$$S_{D3} = 2N\int_{\upsilon_*}^{\infty}\mathrm{d}\upsilon\,\frac{\mu_b^2}{\sqrt{\upsilon^2\mu_b^2(\upsilon) - 2\bar{\mathcal{P}}^2\tilde{f}^{-1}(\upsilon)}} - \frac{\pi N\bar{\mathcal{P}}^2}{Q}\big(\omega\eta_e - \frac{1}{2}\sinh(2\omega\eta_e)\big)\,. \tag{C.14}$$

We note that the integral in the DBI term is logarithmically divergent. As discussed in Section 2.2, we regulate the divergence by introducing an upper cut-off at $\upsilon = \upsilon_{max}$ in the integral and subtracting, for each boundary insertion point, the action of a *vertical* curve with $P_x = P_y = 0$,

$$S^0_{D3} = N\int_{\upsilon_*}^{\upsilon_{max}}\mathrm{d}\upsilon\,\frac{\mu_b(\upsilon)}{\upsilon}\,. \tag{C.15}$$

The integral in (C.12) is finite as it stands and does not require any regularisation.

For given values of the parameters m and Q, that characterise a D5-brane embedding at a particular temperature and charge density, we evaluate the regularised D3-brane

action numerically for different values of the dimensionless parameter $\bar{\mathcal{P}}$. The graphs in Figure 7 are obtained by plotting the result against the dimensionless combination

$$\Delta x\, \bar{M} = \frac{2m\bar{\mathcal{P}}}{Q} \sinh\left(\omega\eta_e\right), \tag{C.16}$$

evaluated at the same parameter values using (C.12).

In Section 2.2 we considered the corresponding calculation at vanishing charge density. The formulae we used there can be obtained by taking the $Q \to 0$ limit at fixed temperature in the formulae in this Appendix. The correct limit is obtained by letting $\omega \to 0$ and $\beta \to \infty$ in (C.13) while keeping the dimensionless parameter $\bar{\mathcal{P}}$ fixed.

By inspecting (C.9), we immediately see that $\bar{\mathcal{P}} \to \bar{P}$ in this limit, where $\bar{P}$ is the dimensionless parameter used in the geodesic calculation in Section 2.2. If we then insert (C.12) into (C.16) and take the limit, we obtain

$$\Delta x\, \bar{M}\Big|_{Q=0} = \frac{4m\bar{P}}{\pi} \int_{\upsilon_*}^{\infty} \mathrm{d}\upsilon\, \frac{1}{\upsilon^2 \tilde{f}(\upsilon)\sqrt{\upsilon^2\mu_b^2(\upsilon) - 2\bar{P}^2\tilde{f}^{-1}(\upsilon)}}, \tag{C.17}$$

which is the same as (2.19) employed in Section 2.2.

We obtain the D3-brane action at vanishing charge density in a similar fashion. The magnetic term in (C.14) vanishes in the $Q \to 0$ limit, as can easily be seen by carrying out a small ω expansion inside the parenthesis,

$$-\frac{\pi N\bar{\mathcal{P}}^2}{Q}\big(\omega\eta_e - \frac{1}{2}\sinh\left(2\omega\eta_e\right)\big) = O(Q^2), \tag{C.18}$$

and the remaining DBI-term reduces to

$$S_{D3}\Big|_{Q=0} = 2N \int_{\upsilon_*}^{\infty} \mathrm{d}\upsilon\, \frac{\mu_b^2(\upsilon)}{\sqrt{\upsilon^2\mu_b^2(\upsilon) - 2\bar{P}^2\tilde{f}^{-1}(\upsilon)}}, \tag{C.19}$$

which is the integral in (2.17) in Section 2.2.

D Asymptotic limits

While the main part of the calculations in this work are numerical, it is nonetheless useful to compare the results to analytic approximations in the appropriate limits. This is especially true on limits where either the parameters or the observables become very large or very small, since it can be hard to predict a priori at what point this causes a breakdown of the numerics.

In what follows, we will carry out such approximations and find that our numerics indeed remains reliable for the whole range of parameters studied. Along the way, we will confirm certain asymptotic behaviours that the numerical calculations already suggest.

D.1 D5 limits

For the D5 backgrounds, we can complement the numerics by calculating the free energy analytically at all corners of the $(T, \bar{\rho})$ -plane. As a matter of fact, the low-temperature case has two distinct limits: one where we first take $T \to 0$ while holding $\bar{\rho}$ constant, in which case $Q \to \infty$, and another, where $\bar{\rho}$, or equivalently Q goes to zero first, and only then do we take $T \to 0$.

D.1.1 High T, zero $\bar{\rho}$

Let us first set $\bar{\rho} = 0$. Now the high-temperature limit for the D5-embedding can be solved semi-analytically, as is done for the D7/D3 system [21]. This is easiest to do in the original coordinate u/u_0, however we present the analysis in the υ coordinates for consistency. High temperature, *i.e.* $\frac{T}{M} \gg 1$, means a very small boundary mass $m \ll 1$, cf. (2.13). Thus, we need to expand $\chi(\upsilon)$ around $\chi = 0$. The resulting linearized equation of motion has the solution

$$\chi(\upsilon) = \chi_{\rm as}(\upsilon) \equiv \frac{1}{\upsilon\sqrt{\tilde{f}(\upsilon)}} \left({}_2F_1\left(\frac{1}{4}, \frac{1}{2}; \frac{3}{4}; \frac{4}{\upsilon^4 \tilde{f}(\upsilon)^2}\right) - \frac{4\sqrt{2}\Gamma\left(\frac{3}{4}\right)^2 \, {}_2F_1\left(\frac{1}{2}, \frac{3}{4}; \frac{5}{4}; \frac{4}{\upsilon^4 \tilde{f}(\upsilon)^2}\right)}{\upsilon\sqrt{\tilde{f}(\upsilon)}\Gamma\left(\frac{1}{4}\right)^2} \right) \tag{D.1}$$

in terms of the hypergeometric function ${}_2F_1$.[13] We fixed the boundary conditions by requiring regularity at the horizon and unit boundary mass [21], that is

$$\chi_{\rm as}(\upsilon) \sim \frac{1}{\upsilon} + \frac{c_{\rm as}}{\upsilon^2} + \dots \,, \qquad \upsilon \to \infty \,. \tag{D.2}$$

The coefficient of the $\frac{1}{\upsilon^2}$ -term at the boundary is $c_{\rm as} = -\frac{4\sqrt{2}\Gamma\left(\frac{3}{4}\right)^2}{\Gamma\left(\frac{1}{4}\right)^2} = -0.64622\ldots$. To have an asymptotic solution corresponding to an arbitrary mass we write $\chi = m\chi_{\rm as}$. For this solution, $c = mc_{\rm as}$.

Expanding the regularised free energy (B.2) for a BHE around $\chi = 0$ we get

$$\begin{aligned} \frac{I_{D5,\rm reg}}{\mathcal{K}T^2} \cong \int_{\upsilon_{min}}^{\infty} \mathrm{d}\upsilon \left\{ \upsilon^2 f\sqrt{\tilde{f}} \left(1 - \chi^2 + \frac{1}{2}\upsilon^2\dot{\chi}^2\right) - \upsilon^2 + \frac{m^2}{2} \right\} \\ + \upsilon_{min}\left(\frac{m^2}{2} - \frac{\upsilon_{min}^2}{3}\right) + mc = m^2\gamma + \upsilon_{min}\frac{m^2}{2} - \upsilon_{min}^3\frac{\tilde{f}^{\frac{3}{2}}(\upsilon_{min})}{3} + mc \end{aligned} \tag{D.3}$$

where γ is the integral

$$\gamma = \int_{\upsilon_{min}}^{\infty} \mathrm{d}\upsilon \left\{ \upsilon^2 f\sqrt{\tilde{f}} \left(-\chi_{\rm as}^2 + \frac{1}{2}\upsilon^2\dot{\chi}_{\rm as}^2\right) + \frac{1}{2} \right\}. \tag{D.4}$$

[13] Notice that in terms of the original coordinates u, the argument in the hypergeometric functions is simply $\frac{u_0^4}{u^4}$.

The integral is finite and can be numerically evaluated with the result $\gamma = 0.4693\ldots$.

Inserting $\upsilon_{min} = 1$, $c = mc_{\rm as}$, and $m = \frac{\bar{M}}{T}$, we obtain

$$\frac{I_{D5,\rm reg}}{\mathcal{K}T^2} \cong -\frac{2\sqrt{2}}{3} + \left(\frac{\bar{M}}{T}\right)^2 \left(\gamma + \frac{1}{2} + c_{\rm as}\right) + \cdots = -\frac{2\sqrt{2}}{3} + 0.323\left(\frac{\bar{M}}{T}\right)^2 + \ldots . \quad \text{(D.5)}$$

At very high temperature, at leading order the rescaled free energy is constant, as can also be seen in Figure 2. Therefore we see that the leading term has a T^2 behaviour, as expected in a conformal field theory [26].

D.1.2 Low T, zero $\bar{\rho}$

We can also obtain the low-temperature limit of the D5-action at zero charge density. The coordinates (2.1) are well suited for this calculation. We fix the point u_m where the brane caps off, and then simply expand the equation of motion and action with respect to the horizon position u_0 and around the Minkowski embedding solution $\chi(u) = u_m/u$.

At the leading order, the only contribution comes from the finite part of the counter-terms, and we get

$$\frac{I_{D5,\rm reg}}{\mathcal{K}T^2} = -\frac{\pi T}{8\bar{M}} + O\left(\frac{T}{\bar{M}}\right)^5 , \quad \text{(D.6)}$$

which shows that the free energy of the Minkowski embedding phase indeed goes smoothly to its $T = 0$ value.

D.1.3 High T, high $\bar{\rho}$

Let us then consider the limit where both T and $\bar{\rho}$ are large. The relevant asymptotic limit is where $\bar{\rho}$ is of the same order as $T^2/\bar{M}^2$, in which case $Q = 2\frac{\bar{M}^2}{T^2}\bar{\rho}$ is finite.

In order to compute the regularised free energy to leading order at large T, we can proceed as before, and use a weak field expansion, that is $\chi \to 0$ (and $m \to 0$). Hence, the regularised free energy (B.2) for high-T, arbitrary Q, and dropping all terms proportional to m, becomes:

$$\frac{I_{D5,\rm reg}}{\mathcal{K}T^2} = \int_1^\infty \mathrm{d}\upsilon \left\{ \frac{\left(\upsilon^4 - 1\right)\sqrt{\frac{Q^2}{\upsilon^4+1} + \frac{1}{\upsilon^4} + 1}}{\upsilon^2} - \upsilon^2 \right\} . \quad \text{(D.7)}$$

The integral can be evaluated explicitly using the change of variable $f(\upsilon)/\bar{f}(\upsilon) =$

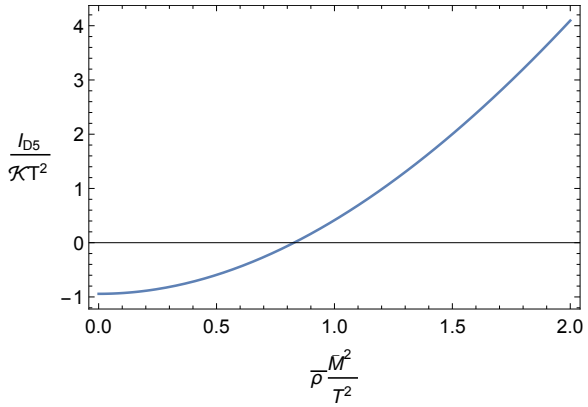

Figure 9: The regularised free energy of the D5-brane at high-T as a function of $\bar{\rho}\frac{\bar{M}^2}{T^2}$.

$\sin y$, with the result

$$\frac{I_{D5,\mathrm{reg}}}{\mathcal{K}T^2} = \frac{1}{3}\left(-\sqrt{2}\sqrt{Q^2+4} - 2\sqrt{iQ}QF\left(i\sinh^{-1}\left(\frac{\sqrt{iQ}}{\sqrt{2}}\right)\middle| -1\right)\right) + O\left(\frac{\bar{M}^2}{T^2}\right), \quad T \gg \bar{M} \tag{D.8}$$

where $F(\phi|k)$ is the elliptic integral of the first kind, with the convention that k, not k^2, appears in the integrand. The expression is real-valued, despite the presence of the imaginary unit, and it agrees with the numerical result in the high-T limit. Figure 9 exhibits the resulting free energy as a function of $\frac{1}{2}Q = \bar{\rho}\frac{\bar{M}^2}{T^2}$.

Finally, in order to characterize the action as a function of the bulk charge, let us note that the asymptotic limits of (D.8) are:

$$\frac{I_{D5,\mathrm{reg}}}{\mathcal{K}T^2} = -\frac{2\sqrt{2}}{3} + \frac{Q^2}{2\sqrt{2}} + O\left(Q^{5/2}\right), \quad Q \ll 1 \tag{D.9}$$

$$\frac{I_{D5,\mathrm{reg}}}{\mathcal{K}T^2} \propto Q^{3/2} + \mathcal{O}(Q), \quad Q \gg 1\,. \tag{D.10}$$

We note that (D.9) matches the leading order of (D.5), as expected.

D.1.4 Low T, finite $\bar{\rho}$

Finally, we consider the case where $T \to 0$ while $\bar{\rho}$ remains finite, in which case $Q \to \infty$. Indeed, this limit needs to be considered since the free energy $I_{D5,\mathrm{reg}}$ diverges at low temperature. The explanation is that the Lorentzian action changes by a finite amount when we go from zero temperature, zero charge, to finite charge, while still keeping

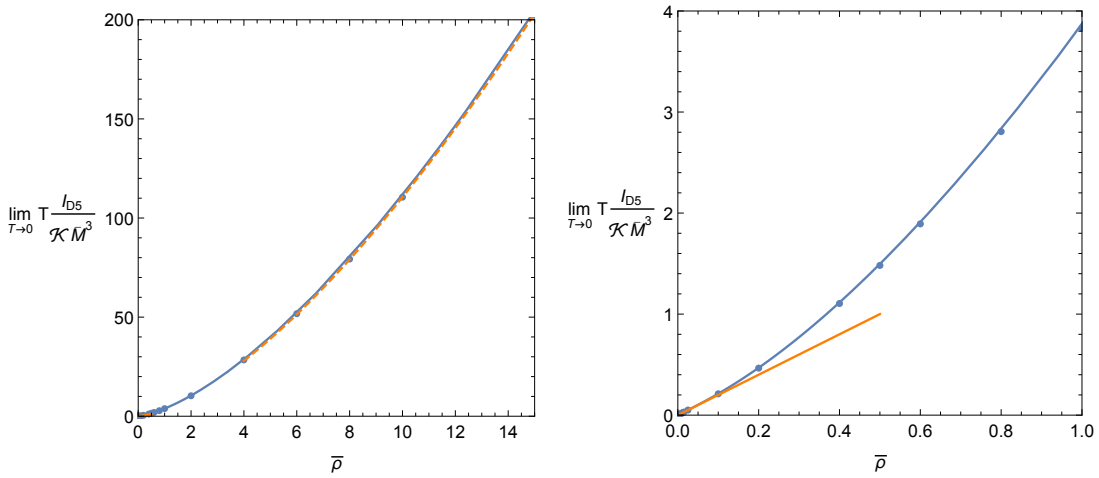

Figure 10: Regularised free energy of charged D5-brane at zero temperature as a function of the boundary charge. The points are evaluated from the smallest-T point available in the finite temperature calculation, whereas the blue curve is from a calculation where the zero-T -limit is first evaluated analytically, as described in the main text. The solid orange curve is the small-$\bar{\rho}$ asymptotic, whereas the the dashed orange curve in the left panel is the the large-$\bar{\rho}$ asymptotic. Right panel shows a closeup of the small-$\bar{\rho}$ -region.

temperature zero. However, in $I_{D5,\mathrm{reg}}$, the Euclidean compactification introduces a factor of $1/T$, and therefore the free energy must indeed diverge as $1/T$ as $T \to 0$ at finite charge.

In terms of field configurations, at finite $\bar{\rho}$, small T, the solution $\chi(\upsilon)$ remains nearly constant up to some finite υ, and eventually breaks away to its asymptotic $m/\upsilon + \ldots$, (2.11), behaviour. As temperature is further decreased, this breakaway point moves to larger and larger υ.

We can explicitly compute $\lim_{T\to 0} TI_{D5,\mathrm{reg}}$, which is finite, by first changing variables to $w = u_0(\upsilon - 1)$. In these coordinates, the asymptotic behaviour appears at a finite value of w. The resulting equations of motion have the large w behaviour $\chi(w) = \hat{m}/w + \hat{c}/w^2 + \ldots$, and we see by comparison to (2.11) that $\hat{m} = mu_0$, $\hat{c} = cu_0^2$. Then $\rho = 1/2N\bar{M}^2\frac{\hat{Q}}{\hat{m}^2}$, where $\hat{Q} = Qu_0^2$. Finally, we expand the free energy with respect to large u_0, keeping $\hat{Q}$ finite, solve numerically the resulting equations of motion with the boundary conditions $\chi(0) = \chi_0$, $\chi'(0) = 0$, and compute the value of $\bar{\rho}$ and the free energy. The boundary condition χ_0 then controls $\bar{\rho}$, whereas the bulk charge $\hat{Q}$ becomes simply a choice of scale, and its actual value is scaled out by a corresponding change in $\hat{m}$. Therefore we set $\hat{Q} = 1$ without loss of generality. The resulting curve is shown in figure 10.

Considering further the limit $\bar{\rho} \to 0$, still at zero temperature, which corresponds

to $\chi_0 \to 1$, we see that the solution tends to almost constant $\chi(w) = 1$ for small w, and then turns sharply to its asymptotic behaviour $\chi(w) \propto 1/w$ for large w. Indeed, $\chi(w) = 1$ is an exact solution to the equation of motion, as is $\chi(w) = \hat{m}/w$ for any $\hat{m}$. In order to move toward a global solution satisfying both of our boundary conditions, let us glue these solutions together at $w = w_s$. In order to avoid a discontinuity, we must then choose $\hat{m} = w_s$. This leaves a discontinuity in the derivative, with a jump of magnitude $1/w_s$. Therefore, the glued function is a (weak) solution in the limit $w_s \to \infty$. Keeping $\bar{\rho} \propto \hat{Q}/w_s^2$ finite, we take that limit and evaluate the free energy, with the result

$$\lim_{T\to 0} \bar{M}^3 T \frac{I_{D5,\mathrm{reg}}}{\mathcal{K}} = 2\bar{\rho}, \quad \text{when } \bar{\rho} \ll 1. \tag{D.11}$$

On the other hand, we can consider the limit $\bar{\rho} \gg 1$ by expanding the regularised free energy and equations of motion around $\chi(w) \sim 0$. The solution to the equation of motion to first order in χ_0 is

$$\chi(w) = -\frac{(-1)^{1/4}\sqrt{\hat{Q}}\chi_0 F\left(\sin^{-1}\left(\frac{(-1)^{3/4}w}{\sqrt{\hat{Q}}}\right)\middle| -1\right)}{w}, \tag{D.12}$$

where $F(\phi|k)$ is as in (D.8), and again, the expression is real. After evaluating the regularised free energy on this solution, we get

$$\lim_{T\to 0} \bar{M}^3 T \frac{I_{D5,\mathrm{reg}}}{\mathcal{K}} = \frac{1}{3}\sqrt{\frac{2}{\pi}}\Gamma^2\left(\frac{1}{4}\right)\bar{\rho}^{3/2}, \quad \text{when } \bar{\rho} \gg 1. \tag{D.13}$$

With these limits we now have analytic control over the D5 free energy in all four corners of the $(T, \bar{\rho})$ -plane, and we find that our numerical results match the approximations in all these cases.

D.2 D3 limits

D.2.1 Large Δx in the black hole embedding

At the limit $\bar{\mathcal{P}} \to \mu_{b,\mathrm{h}}$ the integral in (C.12) and the DBI-term in (C.14) diverge. Therefore this gives the large -Δx limit. The limit $\bar{\mathcal{P}} \to \mu_{b,\mathrm{h}}$ can be approached along two branches: from below, where $\bar{\mathcal{P}} < \mu_{b,\mathrm{h}}$, or from above, where $\bar{\mathcal{P}} > \mu_{b,\mathrm{h}}$. In the first case ($\bar{\mathcal{P}} < \mu_{b,\mathrm{h}}$) the turning point is at the horizon, and we will consider the following double limit: first $\upsilon \to 1$ and then $\bar{\mathcal{P}} \to \mu_{b,\mathrm{h}}$. In the second case, $\bar{\mathcal{P}} > \mu_{b,\mathrm{h}}$, the turning point is υ_*, defined in (2.20), and we will consider the double limit $\upsilon \to \upsilon_*$ first, and then $\upsilon_* \to 1$, which is equivalent to $\bar{\mathcal{P}} \to \mu_{b,\mathrm{h}}$.

To illustrate the computations of the large Δx limit in the BH embedding in a common set-up, we introduce υ_t, which takes value 1 in the $\bar{\mathcal{P}} < \mu_{b,\mathrm{h}}$-branch, and υ_* in

the $\bar{\mathcal{P}} > \mu_{b,\mathrm{h}}$-branch. In both cases the dangerous integrand can be separated as

$$l(\upsilon;\bar{\mathcal{P}}) = \frac{1}{\sqrt{\upsilon^2\mu_b(\upsilon)^2 - 2\bar{\mathcal{P}}^2\tilde{f}^{-1}(\upsilon)}}, \tag{D.14}$$

allowing us to write the DBI -term and the $\omega\eta_e$ integrals as

$$\omega\eta_e = \frac{2Q}{\pi}\int_{\upsilon_t}^{\infty}\frac{l(\upsilon;\bar{\mathcal{P}})}{\upsilon^2\tilde{f}(\upsilon)}\,, \tag{D.15}$$

$$\frac{S_{D3,\mathrm{DBI}}}{N} = 2\int_{\upsilon_t}^{\infty}\mu_b(\upsilon)^2 l(\upsilon;\bar{\mathcal{P}}). \tag{D.16}$$

We can further separate the divergent factor by writing

$$l_1(\upsilon;\bar{\mathcal{P}}) \equiv \frac{1}{\sqrt{\upsilon^2\mu_{b,t}^2 - \frac{2\bar{\mathcal{P}}^2}{\tilde{f}(\upsilon)}}}\,, \qquad l_2(\upsilon,\bar{\mathcal{P}}) \equiv \frac{l(\upsilon;\bar{\mathcal{P}})}{l_1(\upsilon;\bar{\mathcal{P}})}\,, \tag{D.17}$$

where we have defined $\mu_{b,t} = \mu_b(\upsilon_t)$. In the limit we are considering $\mu_{b,t}$ is approaching $\mu_{b,\mathrm{h}}$. If we set $\bar{\mathcal{P}} = \mu_{b,\mathrm{h}}$, $l_1(\upsilon;\bar{\mathcal{P}})$ diverges as $1/(\upsilon-1)$, and therefore the integral diverges. However, $l_2(\upsilon;\bar{\mathcal{P}})$ remains finite even in this case. [14]

There is a slight difference in the form of $l_1(\upsilon;\bar{\mathcal{P}})$ between the two cases, $\bar{\mathcal{P}} < \mu_{b,\mathrm{h}}$ and $\bar{\mathcal{P}} > \mu_{b,\mathrm{h}}$, since in the latter case $\bar{\mathcal{P}}$ must be written in terms of υ_* in order to capture the behavior of the function at υ_*. However, in both cases an antiderivative of $l_1(\upsilon;\bar{\mathcal{P}})$ can be found exactly in terms of the incomplete elliptic integral of the first kind. Denoting the antiderivative as

$$L_1(\upsilon;\bar{\mathcal{P}}) = \int \mathrm{d}\upsilon\; l_1(\upsilon;\bar{\mathcal{P}}) \tag{D.18}$$

for some fixed specific choice of the constant of integration, we can analyze its divergence at $\upsilon = 1$ or $\upsilon = \upsilon_*$, respectively, as $\bar{\mathcal{P}} \to \mu_{b,\mathrm{h}}$. We will find in both cases that $L_1(\upsilon_t;\bar{\mathcal{P}})$ diverges as $\log(|\bar{\mathcal{P}} - \mu_{b,\mathrm{h}}|)$. We want to stress that the divergence in L_1 is characteristic of the limit $\bar{\mathcal{P}} \to \mu_{b,\mathrm{h}}$, $\upsilon_t \to 1$: when $\bar{\mathcal{P}} > \mu_{b,\mathrm{h}}$ and therefore $\upsilon_* > 1$, there is a one-over-square-root –divergence at the lower limit of the integral, which integrates to a finite number. When $\bar{\mathcal{P}} < \mu_{b,\mathrm{h}}$, even the integrand itself is finite at $\upsilon = 1$.

Now we write, for $\bar{\mathcal{P}} \neq \mu_{b,\mathrm{h}}$:

$$\begin{aligned}\omega\eta_e &= \frac{2Q}{\pi}\int_{\upsilon_t}^{\infty}\frac{l_2(\upsilon;\bar{\mathcal{P}})}{\upsilon^2\tilde{f}(\upsilon)}l_1(\upsilon;\bar{\mathcal{P}}) \\ &= \left[\frac{2Q}{\pi}\frac{l_2(\upsilon;\bar{\mathcal{P}})}{\tilde{f}(\upsilon)\upsilon^2}L_1(\upsilon;\bar{\mathcal{P}})\right]\Bigg|_{\upsilon=\upsilon_t}^{\infty} - \frac{2Q}{\pi}\int_{\upsilon_t}^{\infty}\frac{\mathrm{d}}{\mathrm{d}\upsilon}\left(\frac{l_2(\upsilon;\bar{\mathcal{P}})}{\upsilon^2\tilde{f}(\upsilon)}\right)L_1(\upsilon;\bar{\mathcal{P}})\,\mathrm{d}\upsilon\,.\end{aligned} \tag{D.19}$$

[14] Along the two branches the specific values of $l_2(\upsilon;\bar{\mathcal{P}})$ are actually different.

The first term vanishes in the upper limit. Integrating L_1 with respect to υ gives a function of $\bar{\mathcal{P}}$ that is bounded at $\upsilon = \upsilon_t$ for all $\bar{\mathcal{P}} \neq \mu_{b,\mathrm{h}}$, and the other factors in the integral are themselves bounded. Hence, in the limit $\bar{\mathcal{P}} \to \mu_{b,\mathrm{h}}$ the second term in (D.19) will give a finite result. Denoting such remaining integral term as $\frac{2Q}{\pi \tilde{f}(\upsilon_t)\upsilon_t^2} R_{\omega\eta_e}(\bar{\mathcal{P}})$, we can solve

$$l_2(\upsilon_t;\bar{\mathcal{P}})L_1(\upsilon_t;\bar{\mathcal{P}}) = \frac{\pi \tilde{f}(\upsilon_t)\upsilon_t^2}{2Q}\omega\eta_e + R_{\omega\eta_e}(\bar{\mathcal{P}}). \tag{D.20}$$

We do the same integration-by-parts on $S_{D3,\mathrm{DBI}} - S^0_{D3}$ and use the above to write

$$\frac{S_{D3,\mathrm{DBI}} - S^0_{D3}}{N} = \mu_{b,t}^2 \frac{\pi \tilde{f}(\upsilon_t)\upsilon_t^2}{Q}\omega\eta_e + 2\mu_{b,t}^2 R_{\omega\eta_e}(\bar{\mathcal{P}}) - R_{S_{D3}}(\bar{\mathcal{P}}). \tag{D.21}$$

We then insert this into (C.14), using (C.16) to express $\omega\eta_e$ in terms of Δx, to obtain the regularised D3-brane action,

$$\frac{S_{D3,\mathrm{reg}}}{N} = (\tilde{f}(\upsilon_t)\upsilon_t^2\mu_{b,t}^2 - \bar{\mathcal{P}}^2)\frac{\pi}{Q}\,\mathrm{arcsinh}\left(\frac{Q\Delta x\bar{M}}{2m\bar{\mathcal{P}}}\right) + \frac{\pi\bar{\mathcal{P}}}{2m}\Delta x\bar{M}\sqrt{1+\frac{Q^2\Delta x^2\bar{M}^2}{4m^2\bar{\mathcal{P}}^2}} + R(\bar{\mathcal{P}}), \tag{D.22}$$

where

$$R(\bar{\mathcal{P}}) = 2\mu_{b,t}^2 R_{\omega\eta_e}(\bar{\mathcal{P}}) - R_{S_{D3,\mathrm{DBI}}}(\bar{\mathcal{P}})\,. \tag{D.23}$$

This is still an exact result. The key to deriving the large-Δx limit is to now observe that since L_1 has a logarithmic divergence when $\bar{\mathcal{P}} \approx \mu_{b,\mathrm{h}}$, the first terms in (D.20) and (D.21) dominate over the integral terms $R_{\omega\eta_e}$ and $R_{S_{D3,\mathrm{DBI}}}$, which are finite, as explained above. Therefore, at leading order in the limit $\bar{\mathcal{P}} \to \mu_{b,\mathrm{h}}$, the dependence on $\bar{\mathcal{P}}$ comes from the terms in (D.22) that contain Δx, and we obtain

$$\frac{S_{D3,\mathrm{reg}}}{N} \approx \mu_{b,\mathrm{h}}^2\frac{\pi}{Q}\,\mathrm{arcsinh}\left(\frac{Q\Delta x\bar{M}}{2m\mu_{b,\mathrm{h}}}\right) + \frac{\pi\mu_{b,\mathrm{h}}}{2m}\Delta x\bar{M}\sqrt{1+\frac{Q^2\Delta x^2\bar{M}^2}{4m^2\mu_{b,\mathrm{h}}^2}} + R(\mu_{b,\mathrm{h}})\,. \tag{D.24}$$

When $\Delta x\bar{M} \ll \frac{m\mu_{b,\mathrm{h}}}{Q}$ we get

$$\frac{S_{D3,\mathrm{reg}}}{N} \approx \pi T\mu_{b,\mathrm{h}}\Delta x \xrightarrow{T\to\infty} \frac{\pi}{2}T\Delta x, \tag{D.25}$$

and when $\Delta x\bar{M} \gg \frac{m\mu_{b,\mathrm{h}}}{Q}$

$$\frac{S_{D3,\mathrm{reg}}}{N} \approx \frac{\pi Q}{4m^2}\Delta x^2\bar{M}^2 = \frac{\pi}{2}\bar{\rho}\Delta x^2\bar{M}^2. \tag{D.26}$$

Note that when Q is small but non-vanishing, there may be a long range of Δx where the approximation (D.25) is valid before the system crosses over to its asymptotic behavior described by (D.26). At a given charge density and temperature, the crossover occurs at a distance where the two terms inside the square root in (D.24) are equal,

$$\Delta x_{\mathrm{crossover}}\bar{M} = \frac{\mu_{b,\mathrm{h}}T}{\bar{M}\bar{\rho}} \xrightarrow{T\to\infty} = \frac{T}{2\bar{M}\bar{\rho}}. \tag{D.27}$$

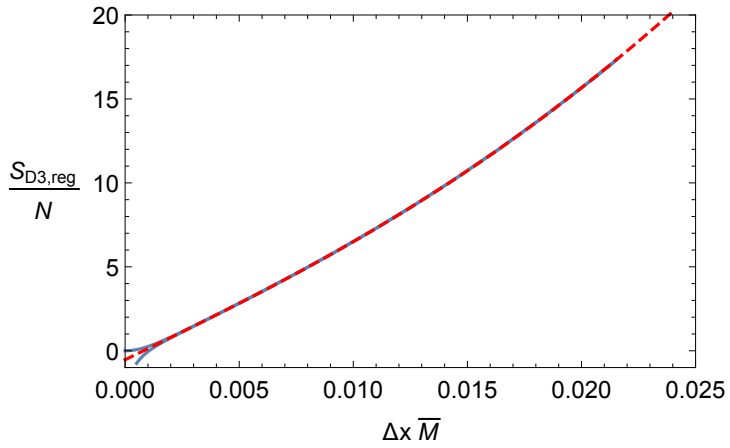

Figure 11: Comparison of our numerical results for the D3-brane action (blue curve) and the approximation (D.24) (dashed red curve) at $\bar{\rho} \approx 13300$ and $\frac{T}{\bar{M}} \approx 422$. These values of $\bar{\rho}$ and T were selected to exhibit the crossover between linear and quadratic dependence on Δx. The constant remainder term $R(\mu_{b,\mathrm{h}})$ was fitted to match the largest Δx achieved by our numerics.

In other words, while the system always asymptotes to a quadratic behaviour at any finite charge, the crossover distance, where this behaviour takes over, diverges as $\bar{\rho}$ goes to zero.

D.2.2 Low-$\bar{\mathcal{P}}$ limit of the D3-brane action

At finite $\bar{\rho}$ and low temperature, the argument of the sinh-term in equations (C.14, C.16) becomes large due to the factor $1/T^2$, and therefore the sinh-term itself becomes extremely large. This means that the most interesting region for Δx is at extremely small values of $\bar{\mathcal{P}}$, to the extent that this region is not directly accessible to numerical calculations using standard tools. In contrast, this region lends itself very well to an analytic low-$\bar{\mathcal{P}}$ approximation. Specifically, let us take $\bar{\mathcal{P}} \ll \mu_{b,\mathrm{h}}$, and expand $\omega\,\eta_e$ to get

$$\omega\eta_e = \int_1^\infty \frac{4\bar{\rho}\bar{M}^2}{\pi\upsilon^3 T^2 \tilde{f}(\upsilon)\mu_b(\upsilon)}\,\mathrm{d}\upsilon + O\left(\frac{\bar{\mathcal{P}}^2}{\mu_{b,\mathrm{h}}^2}\right) = \frac{k}{T^2} + O\left(\frac{\bar{\mathcal{P}}^2}{\mu_{b,\mathrm{h}}^2}\right) \tag{D.28}$$

where we have defined k/T^2 as the integral appearing in (D.28). Note that this is independent of $\bar{\mathcal{P}}$, and especially the sinh-term is independent of $\bar{\mathcal{P}}$ in this approximation. Then we get from (C.16) that

$$\bar{\mathcal{P}} = \frac{\bar{\rho}\bar{M}^2}{T^2 \sinh(\frac{k}{T^2})}\Delta x. \tag{D.29}$$

We then plug this into (C.14), observe that the geometric part is $S^0_{D3}/N + \frac{\pi}{2\bar{\rho}\bar{M}^2}\bar{\mathcal{P}}^2 k$, and simplify to get

$$S_{D3,\mathrm{reg}} \equiv S_{D3} - S^0_{D3} = \frac{\pi\bar{\rho}N}{2}\frac{\Delta x^2\bar{M}^2}{\sinh(\frac{k}{T^2})}\sqrt{1+\sinh^2(\frac{k}{T^2})} + O\left(\frac{\bar{\mathcal{P}}^2}{\mu^2_{b,\mathrm{h}}}\right). \tag{D.30}$$

It is instructive to consider when this limit is valid in terms of Δx. The ratio of the integrands in the leading and next-to-leading terms in (D.28) is $\bar{\mathcal{P}}^2/(\mu_b^2\tilde{f}v^2)$. Approximating μ_b by $\mu_{b,\mathrm{h}}$, making the further approximation that the rest of the integrand can be treated as a constant, integrating, requiring that this ratio is small, and solving the corresponding Δx from (D.29), we get the approximate condition

$$\Delta x\bar{M} \ll \frac{T\sinh(\frac{k}{T^2})\mu_{b,\mathrm{h}}}{\bar{\rho}}. \tag{D.31}$$

Comparing to numerics at not very low T, we see that indeed near this value of Δx the approximation starts to deviate very significantly from the numerical results. We note that in the region where T is low and numerics becomes difficult due to the huge sinh-term, the range of validity increases due to that very same term. Therefore we can trust the approximation to give a very precise picture at low T and moderate Δx.

Finally, we consider the low-T limit,

$$S_{D3,\mathrm{reg}} = \frac{\pi}{2}\,\bar{\rho}\,\bar{M}^2 N\Delta x^2\,, \tag{D.32}$$

and, on the other hand, the zero-charge limit,

$$S_{D3,\mathrm{reg}} = \frac{\pi}{2}\,\frac{T^2}{\bar{k}}\,N\,\Delta x^2\,, \tag{D.33}$$

where $\bar{k} = \frac{k}{\bar{\rho}\bar{M}^2}$.

References

[1] N. Iqbal, *"Monopole correlations in holographically flavored liquids"*, Phys.Rev. D91, 106001 (2015), arxiv:1409.5467.

[2] T. Faulkner and N. Iqbal, *"Friedel oscillations and horizon charge in 1D holographic liquids"*, JHEP 1307, 060 (2013), arxiv:1207.4208.

[3] A. M. Polyakov, *"Compact Gauge Fields and the Infrared Catastrophe"*, Phys. Lett. B59, 82 (1975). • A. M. Polyakov, *"Quark Confinement and Topology of Gauge Groups"*, Nucl. Phys. B120, 429 (1977).

[4] N. Read", *"Spin-Peierls, valence-bond solid, and Néel ground states of low-dimensional quantum antiferromagnets"*, Physical Review B 42, 4568 (1990). • N. Read",

"Valence-bond and spin-Peierls ground states of low-dimensional quantum antiferromagnets", Physical Review Letters 62, 1694 (1989). • G. Murthy and S. Sachdev, *"Action of Hedgehog Instantons in the Disordered Phase of the (2+1)-dimensional CP**(^{1}N) Model"*, Nucl. Phys. B344, 557 (1990).

[5] S. S. Pufu, *"Anomalous dimensions of monopole operators in three-dimensional quantum electrodynamics"*, Phys. Rev. D89, 065016 (2014), arxiv:1303.6125. • S. S. Pufu and S. Sachdev, *"Monopoles in 2 + 1-dimensional conformal field theories with global U(1) symmetry"*, JHEP 1309, 127 (2013), arxiv:1303.3006. • E. Dyer, M. Mezei, S. S. Pufu and S. Sachdev, *"Scaling dimensions of monopole operators in the $\mathbb{CP}^{N_b-1}$ theory in 2 + 1 dimensions"*, JHEP 1506, 037 (2015), arxiv:1504.00368.

[6] S. M. Chester, M. Mezei, S. S. Pufu and I. Yaakov, *"Monopole Operators from the $4-\epsilon$ Expansion"*, arxiv:1511.07108.

[7] V. Borokhov, A. Kapustin and X.-k. Wu, *"Topological disorder operators in three-dimensional conformal field theory"*, JHEP 0211, 049 (2002), hep-th/0206054.

[8] V. G. Filev, *"A Quantum Critical Point from Flavours on a Compact Space"*, JHEP 1408, 105 (2014), arxiv:1406.5498.

[9] S. Bolognesi and D. Tong, *"Monopoles and Holography"*, JHEP 1101, 153 (2011), arxiv:1010.4178. • P. Sutcliffe, *"Monopoles in AdS"*, JHEP 1108, 032 (2011), arxiv:1104.1888. • R. Rougemont, J. Noronha, C. A. D. Zarro, C. Wotzasek, M. S. Guimaraes and D. R. Granado, *"Vanishing DC holographic conductivity from a magnetic monopole condensate"*, JHEP 1507, 070 (2015), arxiv:1505.02442.

[10] O. DeWolfe, D. Z. Freedman and H. Ooguri, *"Holography and Defect Conformal Field Theories"*, arXiv.org 1507, 025009 (2001), hep-th/0111135v3. • J. Erdmenger, Z. Guralnik and I. Kirsch, *"Four-Dimensional Superconformal Theories with Interacting Boundaries or Defects"*, arXiv.org 1507, 025020 (2002), hep-th/0203020v2. • A. Karch and E. Katz, *"Adding flavor to AdS/CFT"*, arXiv.org 1507, E. Katz (2002), hep-th/0205236v2. • K. Skenderis and M. Taylor, *"Branes in AdS and p p wave space-times"*, JHEP 0206, 025 (2002), hep-th/0204054.

[11] S. Sachdev, *"Compressible quantum phases from conformal field theories in 2+1 dimensions"*, arXiv.org 0206, 126003 (2012), arxiv:1209.1637.

[12] E. Witten, *"SL(2,Z) action on three-dimensional conformal field theories with Abelian symmetry"*, hep-th/0307041.

[13] A. Strominger, *"Open P-Branes"*, arXiv.org 0206, A. Strominger (1995), hep-th/9512059v1.

[14] S.-S. Lee, *"Stability of the U(1) spin liquid with spinon Fermi surface in 2+1 dimensions"*, arXiv.org 0206, 085129 (2008), arxiv:0804.3800v3.

[15] N. Evans and E. Threlfall, *"Chemical Potential in the Gravity Dual of a 2+1 Dimensional System"*, Phys. Rev. D79, 066008 (2009), arxiv:0812.3273. • V. G. Filev, *"Hot Defect Superconformal Field Theory in an External Magnetic Field"*,

JHEP 0911, 123 (2009), arxiv:0910.0554. • K. Jensen, A. Karch, D. T. Son and E. G. Thompson, *"Holographic Berezinskii-Kosterlitz-Thouless Transitions"*, Phys. Rev. Lett. 105, 041601 (2010), arxiv:1002.3159.

[16] N. Evans, A. Gebauer, K.-Y. Kim and M. Magou, *"Phase diagram of the D3/D5 system in a magnetic field and a BKT transition"*, Phys. Lett. B698, 91 (2011), arxiv:1003.2694. • G. Grignani, N. Kim and G. W. Semenoff, *"D3–D5 holography with flux"*, Phys. Lett. B715, 225 (2012), arxiv:1203.6162.

[17] J. Casalderrey-Solana, H. Liu, D. Mateos, K. Rajagopal and U. A. Wiedemann, *"Gauge/String Duality, Hot QCD and Heavy Ion Collisions"*, arxiv:1101.0618. • J. Erdmenger, N. Evans, I. Kirsch and E. Threlfall, *"Mesons in Gauge/Gravity Duals - A Review"*, Eur. Phys. J. A35, 81 (2008), arxiv:0711.4467.

[18] A. Karch and L. Randall, *"Localized Gravity in String Theory"*, arXiv.org A35, 061601 (2001), hep-th/0105108v2.

[19] J. Babington, J. Erdmenger, N. J. Evans, Z. Guralnik and I. Kirsch, *"Chiral symmetry breaking and pions in non-supersymmetric gauge / gravity duals"*, Phys. Rev. D69, 066007 (2004), hep-th/0306018.

[20] D. Mateos, R. C. Myers and R. M. Thomson, *"Holographic phase transitions with fundamental matter"*, Phys. Rev. Lett. 97, 091601 (2006), hep-th/0605046.

[21] D. Mateos, R. C. Myers and R. M. Thomson, *"Thermodynamics of the brane"*, JHEP 0705, 067 (2007), hep-th/0701132.

[22] S. Kobayashi, D. Mateos, S. Matsuura, R. C. Myers and R. M. Thomson, *"Holographic phase transitions at finite baryon density"*, JHEP 0702, 016 (2007), hep-th/0611099.

[23] A. Karch, A. O'Bannon and K. Skenderis, *"Holographic renormalization of probe D-branes in AdS/CFT"*, JHEP 0604, 015 (2006), hep-th/0512125.

[24] T. Albash, V. G. Filev, C. V. Johnson and A. Kundu, *"A Topology-changing phase transition and the dynamics of flavour"*, Phys. Rev. D77, 066004 (2008), hep-th/0605088.

[25] J. M. Maldacena, *"The Large N limit of superconformal field theories and supergravity"*, Int. J. Theor. Phys. 38, 1113 (1999), hep-th/9711200, [Adv. Theor. Math. Phys.2,231(1998)].

[26] N. Landsman and C. van Weert, *"Real- and imaginary-time field theory at finite temperature and density"*, Physics Reports 145, 141 (1987), http://www.sciencedirect.com/science/article/pii/0370157387901219.